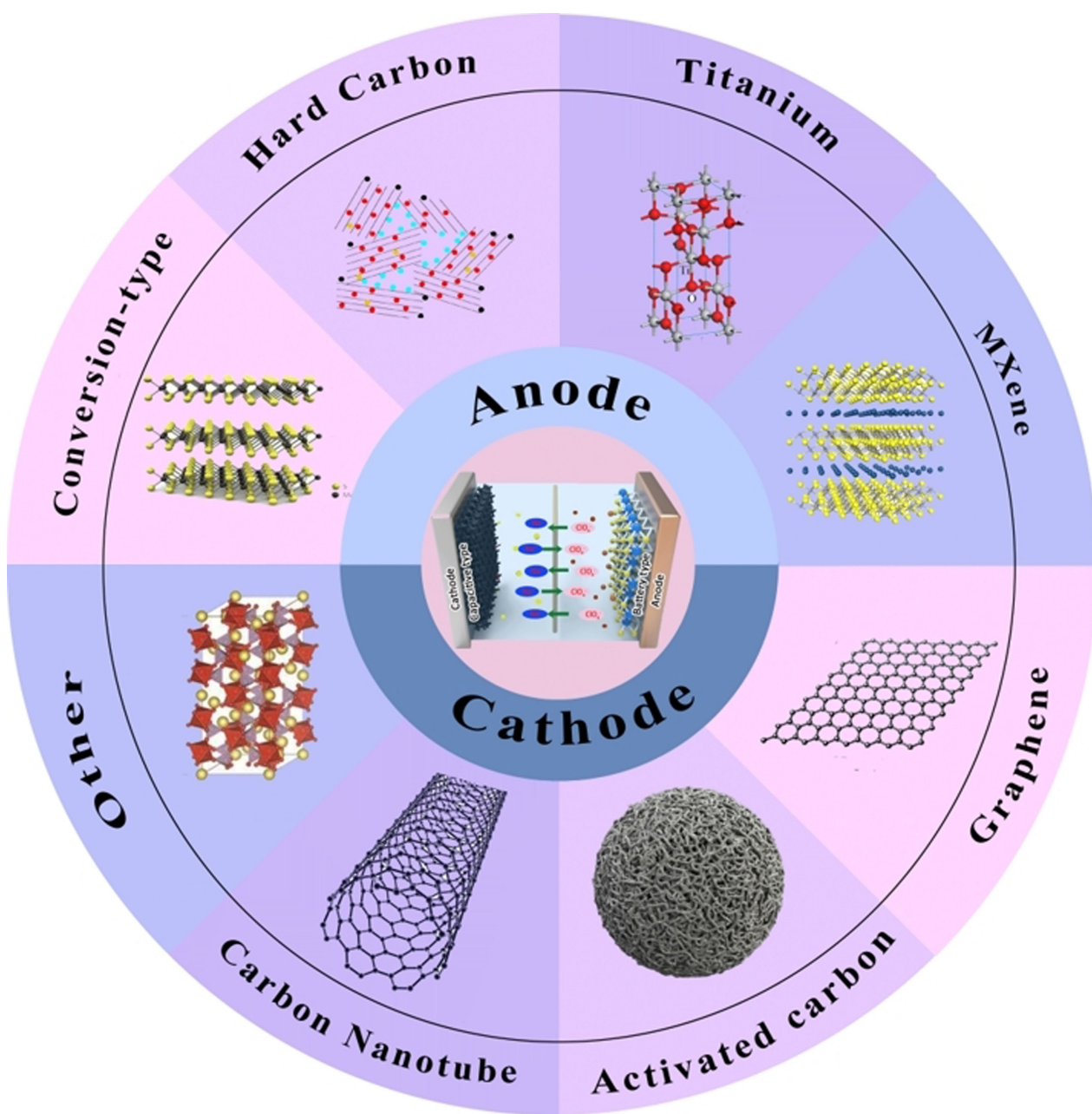


Special
Collection

Sodium-Ion Capacitors: Recent Development in Electrode Materials

Zhihao Zhang,^[a] Zhihao Gu,^[a] Chenguang Zhang,^[a] Jiabao Li,^{*[a]} and Chengyin Wang^{*[a]}



Sodium-ion hybrid capacitors (SICs), combining the advantages of both sodium-ion batteries (SIBs) and electrochemical supercapacitors, have captured sustained attention in the field of energy storage devices due to their high energy and power density, long lifespan, and excellent operation stability. However, conventional SICs based on battery-type anodes and capacitive-type cathodes suffer from imbalance on capacity and kinetics. In this regard, rational structure design on electrode materials is still necessary for SICs. Over the past two decades,

tremendous efforts have been devoted to the exploration of suitable electrode materials to fabricate high-performance SICs. Herein, after a brief introduction on the charge storage mechanisms of SICs, the recent developments on electrode materials for SICs are summarized, especially focusing on material design strategies as well as the relationship between structure and corresponding electrochemical performances. Furthermore, the challenges and opportunities for the further development of SICs are also proposed.

1. Introduction

In recent decades, the rapid consumption of fossil fuels to fulfill the increasing energy demand has resulted in resource depletion and environmental issues, such as global warming and acid rain. In this context, developing clean energy (such as wind energy and solar power) and efficient energy storage systems has become more and more important. Among available energy storage devices, lithium-ion batteries (LIBs) and supercapacitors (SCs), two of the most promising energy storage devices, currently have drawn increasing attention.^[1,2] LIBs, based on ion intercalation/deintercalation in insertion compounds, feature high energy density ($150\text{--}250 \text{ Wh kg}^{-1}$), but suffer from low power density ($<1000 \text{ W kg}^{-1}$) and poor cycling life (<1000 cycles), originating from the sluggish kinetics of Li^+ in the bulk electrode.^[3,4] Comparatively, SCs show advantages in terms of power density ($>10 \text{ kW kg}^{-1}$) and long lifespan (>100000 cycles), resulting from the rapid adsorption/desorption of ions on the surface of electrodes. Unfortunately, the low energy densities ($>10 \text{ Wh kg}^{-1}$) of SCs restrict their applications.^[5,6] In this regard, novel energy storage devices, featuring excellent cycling stability, energy density close to LIBs and power density close to SCs, are extremely desirable. Lithium-ion hybrid capacitors (LICs), combining a battery-type anode and a capacitive-type cathode in lithium-containing electrolyte, possess a higher power density and longer lifespan compared with LIBs, and a higher energy density than that of SCs, which can satisfy the requirements for applications that need the power sources being rapid charged.^[7–10]

Of note, the concerns on the availability and reserves on lithium as well as its uneven distribution have been expressed over the last few years.^[11,12] In this regard, it is urgent to develop alternative electrochemical energy storage devices based on chemical elements that are more abundant than lithium. Due to the high abundance and low cost of sodium resources as well as the identical working mechanism with LIBs,

the last decade has witnessed the rise of sodium-ion batteries both in research and commercialization efforts.^[13–15] Along with the development in batteries, the concept of hybrid capacitor can be also applied to sodium system based on sodium-containing materials and electrolyte.^[16]

As Known, the first LICs based on nano-structured $\text{Li}_4\text{Ti}_5\text{O}_{12}$ (anode) and activated carbon (cathode), was reported in 2001.^[17] While the first study on sodium-ion capacitor (SICs) based on hard carbon (anode) and activated carbon (cathode) was first reported in 2012.^[18] So far, compared with the rapid development of LICs, the research on SICs is still insufficient, and there are many obstacles to be addressed. For example, due to the larger ion radius of sodium (0.102 nm) than that of lithium (0.076 nm), most of the reported electrode materials with excellent lithium storage performance can't be directly employed for SICs without further modification.^[19] Besides, the energy density of SICs is expected to be lower than that of LICs because of the higher redox potential of Na/Na^+ than that of Li/Li^+ , and the sluggish diffusion dynamics of Na^+ in bulk electrode may lead to serious polarization.^[5,20,21] Additionally, the mismatching on capacity and kinetic as well as the unclear coupling mechanism between anode/cathode makes it hard to integrate high energy density, high power density and superior cycling stability in an individual SIC.^[22,23]

To fabricate high-performance SICs, rational design on electrode material is critical. Up to now, few papers have focused on the latest progress of electrode materials for SICs. In this review, the latest advances in nanostructured electrode materials for SICs, including the design and modification of novel nanostructured active materials, are comprehensively reviewed. Firstly, the charge storage mechanism and equations of SICs are introduced. Then we review the recent progress of electrode materials for SICs, and the regulation between the structure/component of electrode materials and corresponding electrochemical performance is also emphasized. Finally, the remaining challenges and suggestions are put forward for the research and future prospects of SICs.

[a] Z. Zhang, Z. Gu, C. Zhang, Dr. J. Li, Prof. C. Wang
School of Chemistry and Chemical Engineering
Yangzhou University
180 Si-Wang-Ting Road, Yangzhou, Jiangsu 225002, China
E-mail: jiabaoli@yzu.edu.cn
wangcy@yzu.edu.cn

An invited contribution to a Special Collection dedicated to Metal-Ion Hybrid Supercapacitors



2. Charge Storage Mechanism and Equations of SICs

Specifically, the operation mechanisms of SICs can be divided into three types: electrolyte consumption, sodium ion ex-

change, and mixed mechanisms based on whether the electrolyte is consumed upon electrochemical cycling, as shown in Figure 1. The details are described as follows.

I) Electrolyte consumption mechanism: the system generally takes carbonaceous materials, metal oxides and Na^+ (de) intercalation compounds as the anode, whereas activated carbon (AC), carbonaceous materials derived from biomass, graphene and carbon nanotubes serve as the cathode. Upon charging, cations and anions are separated to move to the anode and cathode, respectively, due to the action of voltage, which is similar to that of SCs. Instead of simple physical Na^+ adsorption on the electrode surface in SCs, Na^+ intercalates into Na^+ -including compounds or a reduction reaction takes place in the anode of SICs. On the contrary, sodium ions go back from the anode to the electrolyte in the subsequent discharging process. Meanwhile the adsorbed anions are also released from the cathode for charge balance. Typical example of such system is graphite//AC.^[18]

II) Sodium ion migration mechanism: this kind of system usually includes a capacitive-type anode and a battery-type cathode, and the cathode can provide sodium ions. During charging, sodium ions are deintercalated from the cathode, and adsorbed on the surface of anode, and vice versa. Upon electrochemical cycling, the concentration of electrolyte remains unchanged and only serves as a transfer medium for sodium ions. An example of such system is MXene// $\text{Na}_2\text{Fe}_2(\text{SO}_4)_3$.^[25]

III) Mixed mechanism: this type of hybrid capacitor is the combination of the above two types. The most obvious feature

of this type of SICs is that one or both of the electrodes are composed of battery-type and capacitive-type electrode materials. Upon charging, sodium ions are removed from the cathode and enter the electrolyte, while AC in the cathode absorbs anions from the electrolyte. All sodium ions deintercalated from the cathode and provided by electrolyte intercalated into the anode. As for the discharging process, the absorbed anions are released from the AC into the electrolyte to balance the sodium ions deintercalated from anode, while another proportion of Na^+ are inserted into the cathode for the reformation of Na-containing state. An example of such system is $\text{NaTi}_2(\text{PO}_4)_3@\text{rGO}/\text{Na}_3\text{V}_2(\text{PO}_4)_3/\text{C}$ system.^[26]

Generally, energy density and power density are two important characteristics for SICs. For SICs with linear charge/discharge curve, the energy density can be described as follows [Eq. (1)]

$$E = I\Delta t(V_{\min} + V_{\max})/2 \quad (1)$$

where E , I and Δt represent energy density, current density and discharging time, respectively, and V_{\min} and V_{\max} are the minimum and maximum voltages of the SIC.^[28,29]

Actually, the mismatching between the sluggish dynamics of battery-type electrode and the rapid adsorption/desorption of capacitive-type electrode leads to nonlinear curves upon charge/discharge process, which becomes more obvious at higher current density (Figure 2a and b).^[27] In regard of SICs with nonlinear charge/discharge curve, the energy density of SICs is normally estimated through integrating the area below



Zhihao Zhang received his B.S. degree in Polymer Materials and Engineering (2019) from Ludong University. He is currently a master candidate of School of Chemistry and Chemical Engineering, Yangzhou University, China. His research interests are advanced electrode materials for sodium-ion hybrid capacitors.



Zhihao Gu received his B.S. degree in Environmental Engineering (2020) from Yancheng Institute of Technology. He is currently a master candidate of School of Chemistry and Chemical Engineering, Yangzhou University, China. His research focuses on the energy storage materials and devices.



Chenguang Zhang received his B.S. degree in Applied Chemistry (2020) from Nanjing XiaoZhuang University 2019. He is a master candidate of School of Chemistry and Chemical Engineering, Yangzhou University, China. His research is focused on the construction of high-performance metal-ion capacitors.



Dr. Jiabao Li obtained his Ph.D. degree in Materials and Optoelectronic (2020) from East China Normal University (ECNU). He is currently a lecturer in School of Chemistry and Chemical Engineering, Yangzhou University, China. His main research interests are electrochemistry and high-performance electrodes for electrochemical energy storage devices.



Prof. Chengyin Wang received his Ph.D. degree in Physical Chemistry (2007) from Yangzhou University. He is currently a professor in School of Chemistry and Chemical Engineering, Yangzhou University, China. His main research interests focus on the electrochemical sensors and alkalis-ion batteries.



Figure 1. The energy storage mechanisms for SICs. Reproduced from Ref. [24] with permission. Copyright (2020) Wiley-VCH.

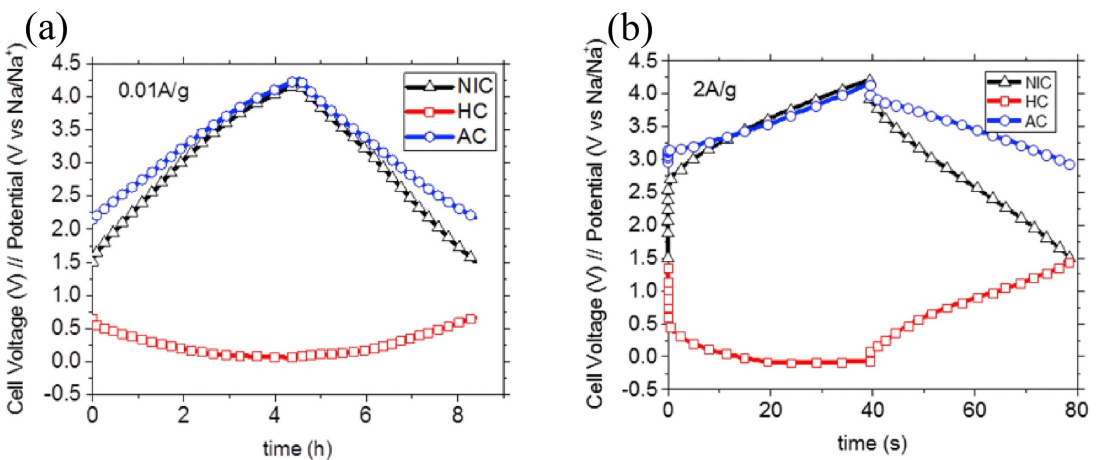


Figure 2. Charge/discharge curves of SICs at 0.01 A g^{-1} (a) and 2.0 A g^{-1} (b). Reproduced from Ref. [27] with permission. Copyright (2017) Elsevier B.V.

the charge/discharge curve based on the following equation [Eq. (2)]:

$$E = I \int V dt \quad (2)$$

where E , I , V and t correspond to the energy density, current density, voltage and discharging time, separately.^[24]

As for the power density, it can be estimated as [Eq. (3)]:

$$P = E / \Delta t \quad (3)$$

where P , E and Δt are power density, energy density and discharging time of the SIC, respectively.^[16,28,29]

Recently, the charge storage based on pseudocapacitance, which arises at the electrode surfaces upon charge transfer, has been proved to be efficient for enhancing the rate capability of target electrode materials.^[6,30–33] Nanostructure fabrication on electrode materials endowed conductive pathways can significantly improve the transport of ions and electrons, thereby leading to enhanced electrochemical performance.^[34–39] Actually, both capacitive and Faradaic reactions contribute to the charge storage in the electrode upon electrochemical cycling.^[40–47] As for SICs, battery-type anodes with feature of capacitive electrochemical behaviors can improve the electrode kinetics and corresponding rate capability, and capacitive-type cathodes with partial Faradaic reaction can increase its specific

capacity, thus resulting in the matching on capacity and kinetics between anode/cathode as well as high energy/power densities of SICs.^[48–50]

Generally, the quantitative analysis of capacitive contribution to the charge storage on the electrode can be calculated based on the following equation [Eq. (4)]:

$$i = av^b \quad (4)$$

in this equation, a and b are both constants, i is the current density at a fixed potential, and v represents the scan rate.^[51,52] Notably, the value of b , a typical index for the kinetics mechanism of charge storage, can be received after modifying Equation (4) into [Eq. (5)]:

$$\log(i) = b \log(v) + \log(a) \quad (5)$$

the b value approaching 1.0 indicates a capacitive dominated electrochemical process, while a value of 0.5 suggests a typical Faradaic reaction-controlled electrochemical process.^[53–55] After plotting $\log(i)$ versus $\log(v)$, the corresponding slope is the value of b . Based on previous studies,^[54,55] the current response at a fixed potential can be separated into capacitive controlled part and Faradaic reaction dominated part, and the relationship between them can be described as follows [Eq. (6)]

$$i_{(V)} = k_1 v + k_2 v^{1/2} \quad (6)$$

where $k_1 v$ and $k_2 v^{1/2}$ correspond to pseudocapacitive and Faradaic contributions, respectively. After further modifying Equation (6) into [Eq. (7)]

$$\frac{i_{(V)}}{v^{1/2}} = k_1 v^{1/2} + k_2 \quad (7)$$

both k_1 and k_2 can be obtained at different voltages, and corresponding contributions from pseudocapacitive and Faradaic reactions are separated at different scan rates.^[56]

3. Materials for SICs

3.1. Anode Materials

Since the study of SICs, a lot of studies have demonstrated that the electrochemical performance of SICs largely depends on the choice of anode materials. To achieve both high energy density and power density as well as long cycling stability in SICs, the anode materials should possess the following merits: 1) low working voltage, resulting in a higher V_{max} of SIC and higher energy/power densities; 2) good rate capability, which allow for high current density and matching with high power cathode; 3) high specific capacity, leading to a long discharge duration (Δt); 4) long lifespan, which is beneficial for the cycling stability.^[24,28,57–59] Herein, several important types of anode materials are described in detail, including carbonaceous anode

materials, MXene-based anode materials, titanium and niobium-based anode materials, and conversion-type anode materials.

3.1.1. Carbonaceous Materials

Due to their outstanding electrical conductivity, abundance in reserve, high chemical stability and tunable structure, carbonaceous materials have shown to be potential candidates for sodium storage.^[60] Particularly, Graphite has been commercialized as anodes for both LIBs and LICs, since it has a low insertion potential (< 0.1 V vs. Li/Li⁺).^[61] However, theoretical calculations and experiments have demonstrated the relatively poor sodium storage performance of graphite in SIBs and SICs because of the larger atomic mass and ionic radius of Na⁺ (22.99, 1.02 Å) than those of Li⁺ (6.94, 0.76 Å).^[29] In view of this, carbonaceous materials with larger tunnels to allow rapid intercalation/deintercalation of Na⁺ should be suitable for SICs.^[62] In contrast, hard carbon (HC), which can be obtained by pyrolysis of high molecular polymer and decomposing a crosslinked block resin, are more suitable as anode materials for SICs owing to its larger interlayer spacing and abundant defect sites.^[63] Based on previous studies,^[64,65] the sodium storage mechanism of hard carbon can be described as: 1) intercalation of Na⁺ between the graphene sheets; 2) sodium storage in the micropores; 3) sodium adsorption on the surface and defect.

Recently, biomass derived carbonaceous materials for efficient sodium storage have attracted increasing attention. As shown in Figure 3a, the peanut shell derived ordered carbon

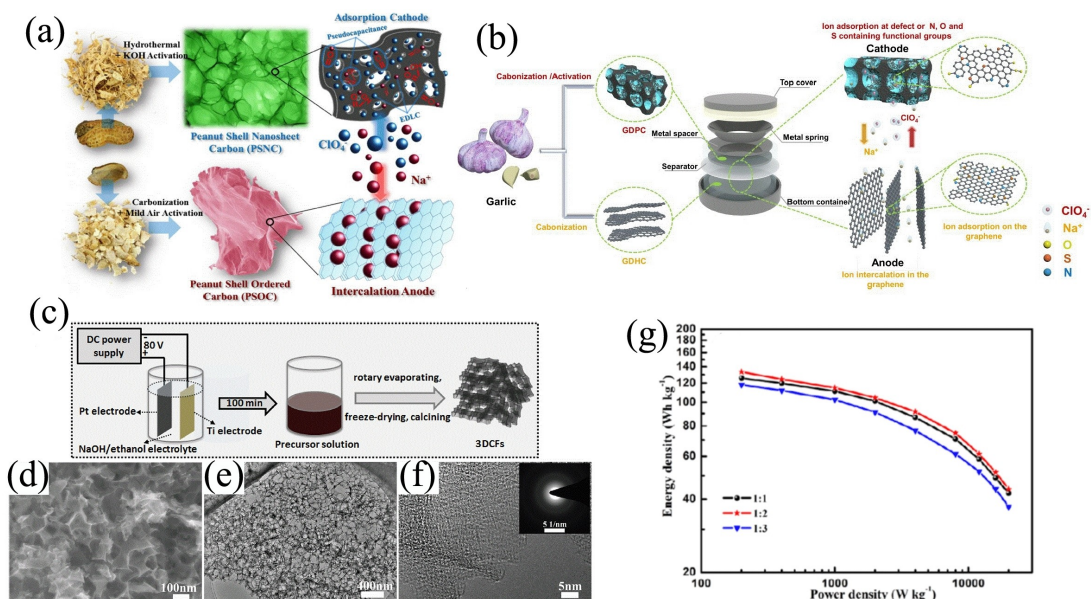


Figure 3. a) Peanut shell derived materials for both cathode and anode as well as their charge storage mechanism in SIC. Reproduced from Ref. [66] with permission. Copyright (2015) The Royal Society of Chemistry. b) Illustration of the preparation process of garlic derived hard carbon and porous carbon as well as mechanism for the sodium storage in SIC. Reproduced from Ref. [67] with permission. Copyright (2019) American Chemical Society. c) Schematic illustration of the fabrication process for the three-dimensional carbon framework (3DCF) and corresponding SEM (d), TEM (e) and HRTEM (f) images (insert of (f) is the corresponding SAED pattern). g) Ragone plots of 3DCF//activated carbon derived from sodium alginate with different mass ratios. Reproduced from Ref. [54] with permission. Copyright (2018) Elsevier B.V.

and carbonaceous nanosheets, which can be employed as intercalation anode and adsorption cathode, manifest excellent electrochemical performances, including both high energy density and power density as well as good cycling stability, which shows the feasibility of the conversion from biomass to electrode materials for SICs.^[66] Besides, Liu et al.^[67] designed well-matched carbonaceous anode and cathode both from garlic (Figure 3b). The garlic derived hard carbon (GDHC) demonstrates high sodium storage performances in half cells. After assembling SIC with GDHC (anode) and garlic derived porous carbon (cathode), the hybrid device exhibits both high energy density and power densities of 156 and 31 Wh kg⁻¹ at 355 and 38910 W kg⁻¹, respectively, and 73% of its initial capacity at 1.5–4.2 V is remained after 10000 cycles.

Table 1 shows the recent developments on the carbonaceous anodes for SICs, from where heteroatom doping and structure design have been proved to be efficient approaches to obtain SICs with both high energy density and power density. Nitrogen, star doping atom, can effectively modulate the electronic structure and charge density distribution when doping into carbonaceous materials. Dong et al.^[68] developed a large-scalable method to prepare the N-doped carbon through employing k-carrageenan as precursor and alkali metal nitrate as activating agent and dopant. Due to the rational design of carbonaceous anode, the optimized SIC, fabricated by the as-prepared sample and methylcellulose derived carbon, exhibits a large energy density of 110.8 Wh kg⁻¹ and capacity retention of 85% after 10000 cycles. What's more, nitrogen, sulfur dual-doping, combining with structure design, is believed to increase the interlayer distance of carbonaceous materials and their sodium ion storage capacity. Wang' group^[69] prepared the nitrogen and sulfur dual-doped carbon nanofiber (S-NCNF) membrane, and the doped S atoms induced an enlarged interlayer distance of 0.38 nm, thus contributing to ion diffusion and charge transfer. Consequently, the fabricated S-NCNF coupled with AC shows high energy density (97 Wh kg⁻¹) and power density (17 kW kg⁻¹) as well as a long cycling life (3000 cycles). Compare with one dimensional nanostructure,

three-dimensional carbon framework (3DCF) with interconnected structure and defective features can efficiently facilitate the sodium diffusion and storage. As shown in Figure 3c, Yan's group^[54] developed an electrolysis method with subsequent calcination approach for the preparation of 3DCF, and corresponding morphology characterizations are shown in Figure 3d-f, where porous structure and rich pores can be clearly seen. The structure advantages inherited from the novel fabrication induce improved electrochemical performances, the optimized hybrid device, based on 3DCF and sodium alginate derived activated carbon with mass ratio of 1:2, displays a high energy density of 133.2 Wh kg⁻¹ at power density of 20.0 kW kg⁻¹ within 0–4.0 V, along with long-term cycling stability up to 4000 cycles (Figure 3g).

3.1.2. MXene-Based Anode Materials

Recently, a new group of 2D transition metal carbides, carbonitrides, and nitrides, labeled as MXene, has attracted wide attention.^[74,75] Generally, the MXene family can be expressed as $M_{n+1}X_nT_x$, where M refers to a transition metal (Ti, Nb, Mn, Mo, Cr, etc.), X is C and/or N, and T_x represents terminal surface groups ($-OH$, $-F$, $-O$, etc.). The typical preparation involves the selectively etching of A layers, such as Al, Si, Ga, etc., from the original $M_{n+1}AX_n$ phases.^[76] Benefiting from their typical 2D structure, superior metallic conductivity, mechanical stability and tunable surface features, MXene has shown promising properties in applications of supercapacitor, rechargeable batteries, hybrid devices, catalysts, oxygen reduction and evolution, and water splitting.^[77]

Due to the well-established etching chemistry, theoretical studies as well as the commercial available precursor, $Ti_3C_2T_x$ is the most studied MXene.^[37,79] Unfortunately, similar to other 2D materials, the stacking issue of $Ti_3C_2T_x$ sheets and sluggish diffusion dynamics within the interlayers are unfavorable for the charge storage in energy storage devices.^[80] Particularly, a lot of modification strategies on $Ti_3C_2T_x$ have been carried out

Table 1. A summary of SICs devices based on carbonaceous anode materials.

Anode//Cathode	Electrolyte	Voltage window	Energy and power densities	Cycling performance	Year	Ref.
Electrochemically exfoliated graphite//AC	1 M NaPF ₆ in DEGDME	1.0–4.3 V	90 Wh kg ⁻¹ at 2000 W kg ⁻¹ 17 Wh kg ⁻¹ at 17500 W kg ⁻¹	100% after 700 cycles at 0.5 A g ⁻¹	2020	[70]
Carbon nanosheet//AC	1 M NaClO ₄ in EC/DMC	1.0–4.0 V	135 Wh kg ⁻¹ at 25000 W kg ⁻¹ 250 Wh kg ⁻¹ at 69 W kg ⁻¹	71.8% after 4000 cycles at 2.0 A g ⁻¹	2020	[71]
Graphite-Sn//AC	1 M NaPF ₆ in DIGLYME	0–4.0 V	~93 Wh kg ⁻¹ at 495 W kg ⁻¹ 33 Wh kg ⁻¹ at 7800 W kg ⁻¹	80% after 8000 cycles at 1.0 A g ⁻¹	2020	[72]
N/P dual-doped carbon nanofiber//AC	1 M NaClO ₄ in DC/EC	0–4.0 V	10.6 Wh kg ⁻¹ at 20000 W kg ⁻¹	77.8% after 10000 cycles at 2.0 A g ⁻¹	2019	[63]
N/S co-doped nanotube-like carbon//AC	1 M NaClO ₄ in EC/DMC	0–2.5 V	100.2 Wh kg ⁻¹ at 250 W kg ⁻¹ 50.69 Wh kg ⁻¹ at 12500 W kg ⁻¹	72% after 1500 cycles at 2.0 A g ⁻¹	2019	[65]
N/S co-doped hierarchical hollow carbon//AC	1 M NaClO ₄ in EC/DMC	2.5–4.5 V	116.4 Wh kg ⁻¹ at 200 W kg ⁻¹ 48.2 Wh kg ⁻¹ at 20000 W kg ⁻¹	92% after 2000 cycles at 2.0 A g ⁻¹	2018	[63]
N doped hollow carbon nanowires//AC	1 M NaClO ₄ in EC/DEC	0.5–4.0 V	108 Wh kg ⁻¹ at 114 W kg ⁻¹ 37.5 Wh kg ⁻¹ at 9000 W kg ⁻¹	70% after 2000 cycles at 2.0 A g ⁻¹	2018	[69]
Nanotube-like hard carbon derived from polyaniline//AC	1 M NaClO ₄ in EC/DEC	1.5–3.5 V	133.0 Wh kg ⁻¹ at 2850 W kg ⁻¹	82.5% after 12000 cycles at 2.0 A g ⁻¹	2017	[62]
N and O functionalized carbon//AC	1 M NaClO ₄ in EC/DEC	0–4.0 V	100.9 Wh kg ⁻¹ at 14250 W kg ⁻¹ 111 Wh kg ⁻¹ at 67 W kg ⁻¹ 38 Wh kg ⁻¹ at 14550 W kg ⁻¹	90% after 5000 cycles at 6.4 A g ⁻¹	2016	[73]

to improve their electrochemical performance on sodium storage. To take full advantage of the electrochemical energy storage capability of $Ti_3C_2T_x$, Zhao et al.^[78] reported the processing of 2D MXene flakes into hollow spheres with 3D architecture via a template method, and Figure 4a and b show the corresponding SEM images, from where uniform hollow spheres can be detected, thus demonstrating the successful fabrication. Electrochemical tests manifest that the 3D MXene exhibits improved sodium storage performance compared with multilayer MXenes and MXene/carbon hybrid in term of capacity, rate capability and cycling stability. Besides, another study from the same group reported the fabrication of bistacked 2D $Ti_3C_2T_x$ MXene, which can be directly employed without electrode fabrication process containing binder, conductive agent and current collector.^[75] Figure 4c illustrates the synthesis process of the $Ti_3C_2T_x$ MXene using HF– H_2SO_4 etchant and the fabrication of bistacked MXene film via vacuum-assisted filtration. Particularly, the hybrid capacitor combining the bistacked MXene (anode) and AC (cathode) demonstrates a

high energy density of 39 Wh kg^{-1} at 1 C rate, and capacity retention of $\sim 60\%$ at 60 C rate compared with its original performance.

To improve the Na^+ transfer kinetics within the interlayers of $Ti_3C_2T_x$ MXene, Liu et al.^[74] reported a novel nitrogen-doped $Ti_3C_2T_x$ MXene and employed as battery-type anode for SICs, introducing the in situ polymeric sodium dicyanamide to optimize the surface terminations. Figure 4d illustrates the corresponding fabrication process. The in-situ formed sodium tricyanomelamine (Na₃TCM) on MXene and high doping content of 5.6 at.% endow the composite with high energy density (97.6 Wh kg^{-1}), high power output (16.5 kW kg^{-1}), and excellent cycling stability (82.6% capacitance retention after 8000 cycles) after coupling with AC in SIC and optimizing the mass ratio between anode and cathode. Figure 4e–f display the corresponding CV curves with different mass ratios at 20 mV s^{-1} and the comparison of Ragone plots between assembled SIC and other MXene based LICs and SICs, which highlights its excellent electrochemical performance. Recently, the interest

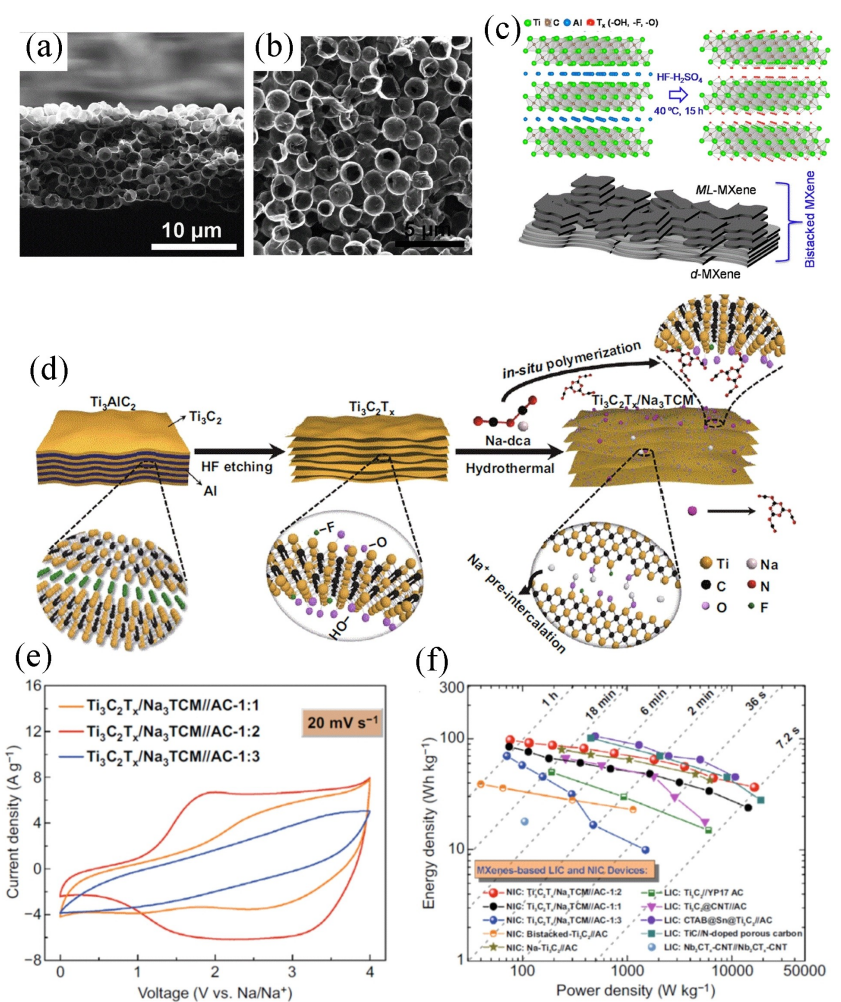


Figure 4. Cross-section (a) and top-view (b) SEM images of 3D microporous $Ti_3C_2T_x$ film. Reproduced from Ref. [78] with permission. Copyright (2017) Wiley-VCH. c) Illustration of the preparation of multilayer $Ti_3C_2T_x$ MXene and corresponding bistacked MXene film through vacuum filtration. Reproduced from Ref. [75] with permission. Copyright (2018) American Chemical Society. Illustration of the synthesis of the $Ti_3C_2T_x$ /sodium tricyanomelamine (d) and corresponding CV curves (e) based on various anode/cathode ratio (1:1, 1:2, 1:3) at a scan rate of 20 mV s^{-1} . Ragone plots (f) of the $Ti_3C_2T_x$ /sodium tricyanomelamine compared with the reported MXene-based LICs and SICs. Reproduced from Ref. [74] with permission. Copyright (2020) The Authors.

on fabrication of customized electrode structure through 3D printing technology has grown due to its facile and large-scale features, from where the 3D structure can induce convenient transfer of ions and electrons, thus contributing to improved electrochemical performances. Sun et al.^[77] demonstrated a 3D-printed SIC based on nitrogen-doped MXene ($\text{N}-\text{Ti}_3\text{C}_2\text{T}_x$) and AC. The well-defined porous structure and uniform nitrogen doping endow the 3D-printed SIC with a large areal mass loading of 15.2 mg cm^{-2} , harvesting areal energy/power densities of 1.18 mWh cm^{-2} and 40.15 mW cm^{-2} , respectively. As shown above, morphology optimization and interlayer engineering are two of the most promising approaches to improve the electrochemical performances of MXene in SICs.^[76,81] Besides, more information of MXene-based anode materials for SIC can be found in Table 2.

3.1.3. Titanium and Niobium-Based Anode Materials

In recent years, titanium-based electrodes have captured increasing attention due to their appropriate working potential, small strain expansion, rapid rate capability and environmental friendliness.^[87–89] Generally, the titanium-based materials can be mainly divided into oxides and non-oxides, from where the former mainly includes TiO_2 , $\text{Na}-\text{Ti}-\text{O}$ compounds, phosphates and other emerging oxide materials, while the latter includes carbides, sulfides and tellurides.^[90] Among them, TiO_2 is a promising battery-type anode for SICs owing to its open framework, which can allow the rapid insertion/extraction of Na^+ upon electrochemical cycling.^[91,92] Besides, depending on the connection method of TiO_6 octahedra, the crystal polymorphs of TiO_2 can be divided into anatase, rutile, brookite, bronze, hollandite, and amorphous phases.^[84,93] Unfortunately, the low electrical conductivity (electronic bandgaps of 3.0–3.2 eV) of TiO_2 and long diffusion length of ion in bulk materials lead to unsatisfied electrochemical performance.^[93,94] Based on literature review of TiO_2 based anodes for SICs,^[59,95–97] interface engineering, fabricating nano-structured TiO_2 , and coupling with conductive support have been proved to be efficient strategies to improve the electrochemical performance of TiO_2 in SICs.

For example, Feng et al.^[84] reported an interface-engineered TiO_2 nanosheets consisting of bronze (~15%) and anatase (~

85%) crystallites (~10 nm), as shown in Figure 5a. The SIC integrated the hierarchical TiO_2 nanosheet anode and an AC cathode displays a high energy density of 200 Wh kg^{-1} and a power density of 6191 W kg^{-1} (Figure 5b). Comparison on the sodium storage performance of TiO_2 nanosheet with other TiO_2 polymorphs possessing various morphologies indicates that the dual-phase TiO_2 nanosheets exhibit the highest specific capacities at all current densities (Figure 5c). Specially, such high performance should be mainly ascribed to the nanointerface between bronze and anatase crystallites induced enhanced pseudocapacitive intercalation of Na^+ (Figure 5a), thus highlighting the advantage of nano-structure fabrication and interface engineering. In regard to the combination with conductive agent, Yan's group^[85] coupled $\text{TiO}_2/\text{carbon}$ nanocomposite (TiO_2/C) anode with a 3D nanoporous carbon cathode, which are both derived from metal-organic frameworks (Figure 5d). Benefiting from the structure advantages of the two electrodes, the coupling between capacity and kinetics are significantly improved, which demonstrates both high energy density (142.7 Wh kg^{-1}) and power output (25 kW kg^{-1}) as well as outstanding cycling stability (90% capacity retention after 10000 cycles). Additionally, Zhou's group^[86] fabricated $\text{TiO}_2@\text{carbon nanotubes}@C$ ($\text{TiO}_2@\text{CNT}@C$) through electrospinning method, which exhibits excellent cyclic stability and excellent rate capability in half cells. Moreover, the SIC, utilizing $\text{TiO}_2@\text{CNT}@C$ as intercalation-type anode and biomass derived porous carbon as capacitive-type cathode, demonstrates an exceptionally high energy density of 81.2 Wh kg^{-1} and a high power density of 12400 W kg^{-1} within 1.0–4.0 V, along with 85.3% capacity retention after 5000 cycles at 1.0 A g^{-1} (Figure 5e-g). Notably, the introduction of carbon nanotubes can dramatically improve the transfer dynamics of ions/electrons in the composite, thus contributing to the enhanced performance in SIC.

Similarly, sodium titanite oxides featuring rich types, low cost and low toxicity have been studied as anode materials for SICs.^[59,91,98] Babu et al.^[99] synthesized the layered sodium titanium oxide hydroxide ($\text{Na}_2\text{Ti}_2\text{O}_4(\text{OH})_2$) through hydrothermal method, which shows superior electrochemical performances in both half cells and assembled SIC. Specifically, the hybrid device coupled with porous carbon demonstrates a maximum energy density of $\sim 65 \text{ Wh kg}^{-1}$ (at 500 W kg^{-1} , 0.2 A g^{-1}) and with more than 93% capacity retention after 3000 cycles. As

Table 2. A summary of SICs devices based on MXene-based anode materials.

Anode//Cathode	Electrolyte	Voltage window	Energy and power densities	Cycling performance	Year	Ref.
Pre-sodiated $\text{Ti}_3\text{C}_2\text{T}_x$ MXene//AC	1 M NaPF_6 in EC/DEC	0.8–3.3 V	249 Wh kg^{-1} at 124.5 W kg^{-1}	–	2021	[76]
$\text{Ti}_3\text{C}_2\text{T}_x/\text{Na}_3\text{TCM}$ //AC	1 M NaPF_6 in EC/DEC	0–4.0 V	97.6 Wh kg^{-1} at 76 W kg^{-1} 36.6 Wh kg^{-1} at 16500 W kg^{-1}	82.6% after 8000 cycles at 4.0 A g^{-1}	2020	[74]
$\text{CT-S@Ti}_2\text{CT}_x$ //AC	1 M NaPF_6 in EC/DEC	1.0–3.8 V	114.0 Wh kg^{-1} at 237 W kg^{-1} 52.6 Wh kg^{-1} at 8240 W kg^{-1}	73.3% over 10000 cycles at 2.0 A g^{-1}	2019	[82]
$\text{Na-Ti}_3\text{C}_2$ //AC	1 M NaClO_4 in EC/PC	3.0–4.2 V	80.2 Wh kg^{-1} at 237 W kg^{-1} 42.2 Wh kg^{-1} at 6127 W kg^{-1}	78.4% after 15000 cycles at 2.0 A g^{-1}	2018	[83]
Bistacked $\text{Ti}_3\text{C}_2\text{T}_x$ MXene//AC	1 M NaPF_6 in EC/DEC	3.0–4.5 V	23 Wh kg^{-1} at 1140 W kg^{-1}	84.2% after 4000 cycles at 2.0 A g^{-1}	2018	[75]
Ti_2C MXene//Alluaudite $\text{Na}_2\text{Fe}_2(\text{SO}_4)_3$	1 M NaPF_6 in EC/DEC	0.1–3.8 V	320 Wh kg^{-1} at 360 W kg^{-1} 260 Wh kg^{-1} at 1400 W kg^{-1}	–	2015	[25]

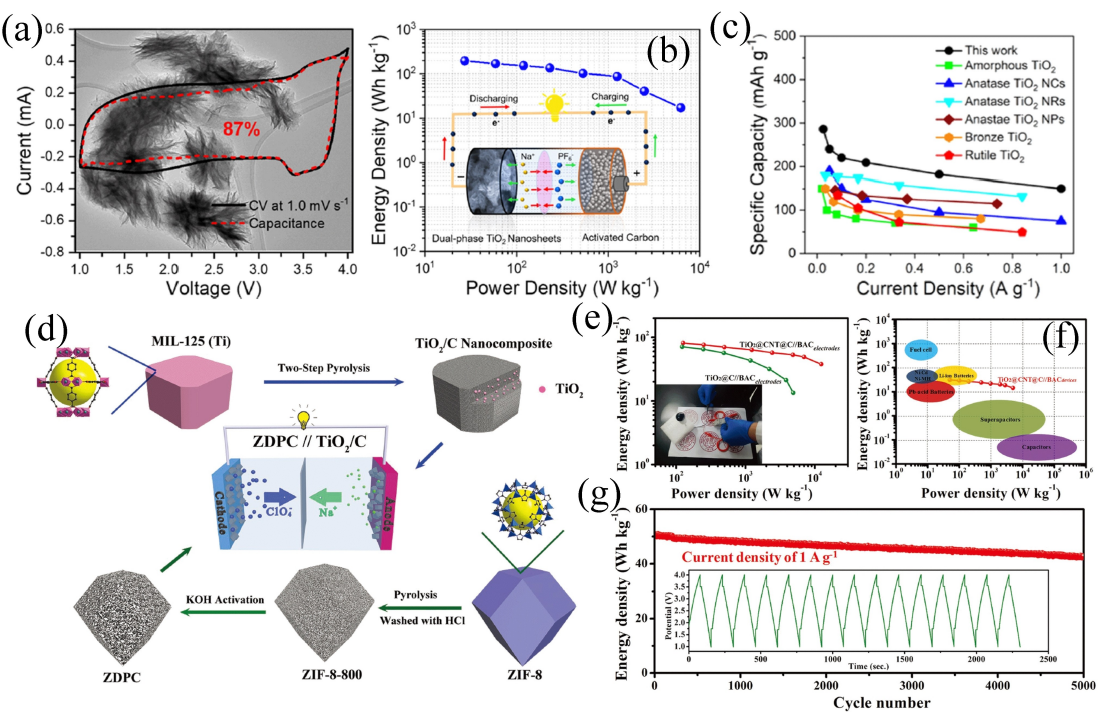


Figure 5. a) TEM image and corresponding CV curves of the dual-phase TiO₂ nanosheets. b) Ragone plot of dual-phase TiO₂ nanosheets//AC. c) Comparison of specific capacity of TiO₂ nanosheet anodes with other TiO₂ polymorphs. Reproduced from Ref. [84] with permission. Copyright (2020) American Chemical Society. d) Schematic illustration showing the construction of SIC using TiO₂/C composite and porous carbon derived from MIL-125 and ZIF-8 (d). Reproduced from Ref. [85] with permission. Copyright (2018) Wiley-VCH. The SIC performances based on TiO₂@carbon nanotubes@C/biomass derived AC: e) Ragone plots; f) device-based performance for the currently available energy-storage systems; g) long cycling performance at 1.0 A g⁻¹. Reproduced from Ref. [86] with permission. Copyright (2017) Wiley-VCH.

shown in Table 3, the various anodes based on TiO₂ and sodium titanite oxides with remarkable electrochemical performances in SICs have been listed, further highlighting the potential of titanium-based anodes for high-performance SICs.

In addition to titanium-based materials, niobium-based compounds are also hot topics in the research of anode materials for SICs.^[104,105] Specifically, orthorhombic Nb₂O₅ (T-Nb₂O₅) has been considered as promising anode for efficient

Table 3. A summary of SICs devices based on titanium-based anode materials.

Anode//Cathode	Electrolyte	Voltage window	Energy and power densities	Cycling performance	Year	Ref.
Oxygen vacancy rich TiO ₂ /carbon nanofibers//AC	1 M NaClO ₄ in EC/DEC	1–4.0 V	91 Wh kg ⁻¹ at 165 W kg ⁻¹ 43.4 Wh kg ⁻¹ at 13000 W kg ⁻¹	71 % after 5000 cycles at 10 A g ⁻¹	2021	[95]
Reduced graphene oxide/TiO ₂ //AC	1 M NaClO ₄ in EC/DMC	1–4.0 V	94 Wh kg ⁻¹ at 200 W kg ⁻¹ 30.6 Wh kg ⁻¹ at 100000 W kg ⁻¹	80 % after 2500 cycles at 3.2 A g ⁻¹	2018	[97]
Mo _{0.1} Ti _{0.9} O ₂ //AC	1 M NaPF ₆ in EC/DEC	1–3.0 V	60 Wh kg ⁻¹ at 350 W kg ⁻¹ 13 Wh kg ⁻¹ at 10650 W kg ⁻¹	75 % after 3000 cycles at 5.0 mA cm ⁻²	2018	[100]
MXene derived TiO ₂ /rGO//PDPC	1 M NaClO ₄ in EC/DEC/FEC	1–4.0 V	94.7 Wh kg ⁻¹ at 247 W kg ⁻¹ 30.9 Wh kg ⁻¹ at 4093 W kg ⁻¹	64 % after 2000 cycles at 2.0 A g ⁻¹	2018	[96]
NaTi ₂ (PO ₄) ₃ //graphene nanosheets	1 M NaClO ₄ in EC/DMC	0–3.0 V	80 Wh kg ⁻¹ at 8000 W kg ⁻¹	90 % after 75000 cycles at 4.0 A g ⁻¹	2017	[98]
Mesoporous TiO ₂ /Graphene//AC	1 M NaClO ₄ in EC/PC/FEC	1–4.0 V	64.2 Wh kg ⁻¹ at 56.3 W kg ⁻¹ 25.8 Wh kg ⁻¹ at 1357 W kg ⁻¹	90 % after 10000 cycles at 10 C	2017	[93]
NaTi ₂ (PO ₄) ₃ mesocrystals//AC	1 M NaClO ₄ in PC	0–2.5 V	56 Wh kg ⁻¹ at 39 W kg ⁻¹ 31 Wh kg ⁻¹ at 4096 W kg ⁻¹	100 % after 20000 cycles at 5.0 A g ⁻¹	2017	[98]
TiO ₂ /carbon fiber cloth//carbon fibers	1 M NaPF ₆ in EC/DMC/EMC	1–4.3 V	73.8 Wh kg ⁻¹ at 550 W kg ⁻¹ 20.5 Wh kg ⁻¹ at 13570 W kg ⁻¹	90 % after 4000 cycles at 1.0 A g ⁻¹	2017	[95]
3D-Na ₂ Ti ₃ O ₇ sheets//graphene foam	1 M NaClO ₄ in EC/DMC	1–3.0 V	55 Wh kg ⁻¹ at 200 W kg ⁻¹ 25.8 Wh kg ⁻¹ at 1357 W kg ⁻¹	80 % after 2500 cycles at 0.5 A g ⁻¹	2016	[101]
Na ₂ Ti ₃ O ₇ @CNT//AC	1 M NaClO ₄ in EC/PC with 5% FEC	0–3.0 V	58.5 Wh kg ⁻¹ at 300 W kg ⁻¹ 21.6 Wh kg ⁻¹ at 3000 W kg ⁻¹	77 % after 4000 cycles at 0.4 A g ⁻¹	2013	[59]

sodium storage due to its large interlayer distance of 0.39 nm in (001) lattice plane and pseudocapacitive feature.^[106] However, similar to titanium-based materials, Nb_2O_5 -based electrodes suffer from their low electrical conductivities.^[107] Generally, the micro/nanostructures of Nb_2O_5 -based electrodes also play important roles for their electrochemical performances, and improved electrochemical performances have been obtained after the combination with carbonaceous materials.^[89,104]

For instance, Tong et al. demonstrated a facile method including two-step hydrolysis synthesis to prepare the sandwich-like mesoporous Nb_2O_5 /graphene/mesoporous Nb_2O_5 ($\text{G}@\text{mNb}_2\text{O}_5$).^[102] Figure 6a-d show the TEM investigations of $\text{G}@\text{mNb}_2\text{O}_5$, where mesoporous Nb_2O_5 layers decorated on graphene are constructed by several nanometer-sized Nb_2O_5 particles. The structural features enable the fabricated SIC, using the sandwich-like composite (anode) and AC (cathode), with a high energy density of 56.1 Wh kg⁻¹ at 120 W kg⁻¹ as well as a high capacity retention of 89% at 1.0 A g⁻¹. Recently, Li et al.^[103] designed the mesoporous T- Nb_2O_5 /carbon nano-

fiber (CNF) networks via in-situ SiO_2 -etching, and the typical preparation process of T- Nb_2O_5 /CNF has been shown in Figure 6e. Notably, the obtained T- Nb_2O_5 /CNF membranes are mechanically flexible without any addition of conductive agent and binder, enabling the fabrication of flexible SIC. Consequently, the electrochemical tests (Figure 6f-h) show superior electrochemical performance in a flexible SIC fabricated by T- Nb_2O_5 /CNF and graphene framework/mesoporous carbon nanofiber (GF/mCNF), delivering an ultrahigh power density of 60 kW kg⁻¹ at 55 Wh g⁻¹. Besides, studies on Nb_2O_5 nanosheet, $\text{Ti}_2\text{Nb}_2\text{O}_9$ nanosheet and core-shell structured $\text{Nb}_2\text{O}_5@$ carbon as anodes for SICs have also shown impressive electrochemical performances.^[89,102-108]

3.1.4. Conversion-Type Anode Materials

As known, multi-electron transfers are involved in the sodium storage process of conversion-type anode materials, thus

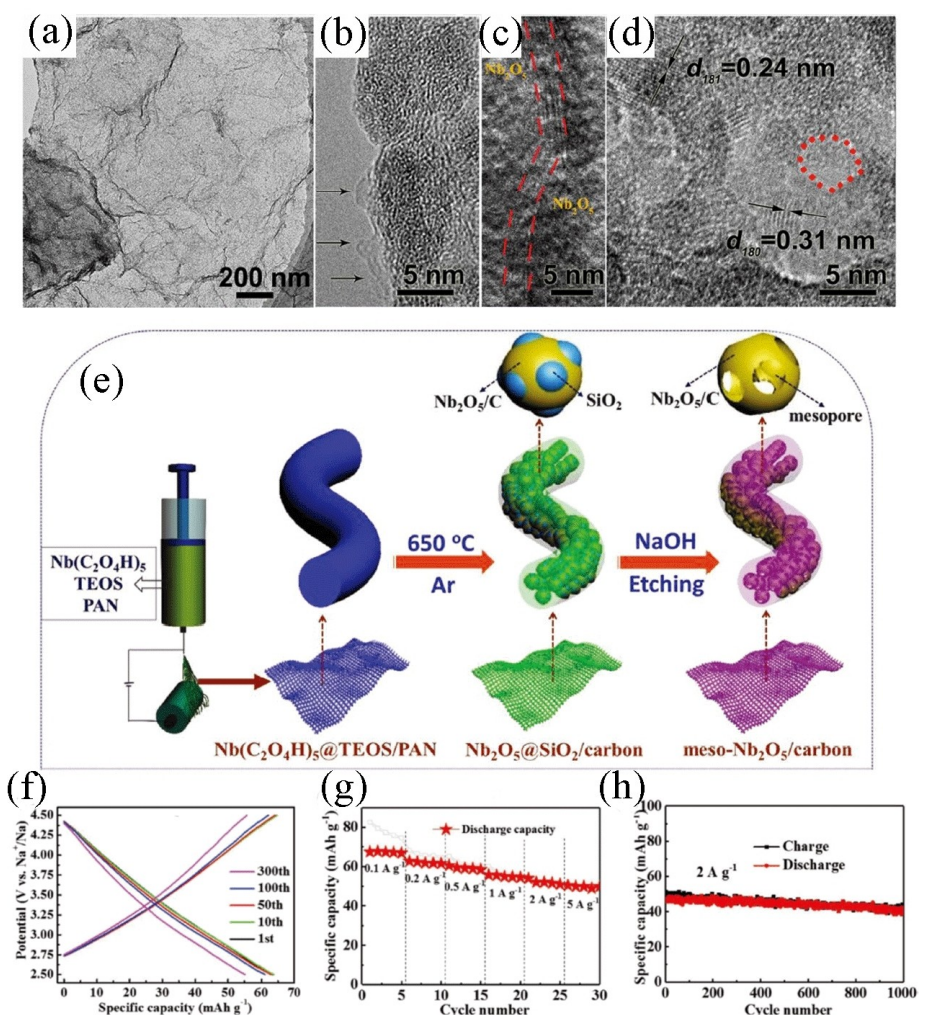


Figure 6. a, b) TEM images, c, d) cross-sectional and top-view HRTEM images of mesoporous Nb_2O_5 /graphene/mesoporous Nb_2O_5 . Reproduced from Ref. [102] with permission. Copyright (2017) Elsevier B.V. e) Illustration of preparation of mesoporous T- Nb_2O_5 /carbon nanofiber film (m- Nb_2O_5 /CNF). The electrochemical performances of SIC based on m- Nb_2O_5 /CNF and graphene framework/mesoporous carbon nanofiber: f) charge/discharge curves at 0.2 A g⁻¹, g) specific capacities at different current densities, and h) the cycling performance at 2.0 A g⁻¹. Reproduced from Ref. [103] with permission. Copyright (2019) Wiley-VCH.

offering high specific capacities.^[41,112–114] The chemical formula of conversion-type anode materials can be denoted as MX, where M corresponds to transition metal, and X represents element such as O and S.^[115,116] Compared with metal oxides, metal sulfides with weak M–S bonds are believed to improve the kinetics of conversion reaction, and have been widely studied as host materials for sodium ions.^[47,49,117–119]

Among the available metal sulfides, molybdenum sulfides (MoS_2), a typical layered transition metal sulfide, possess a large interlayer distance, weak van der Waals force and high theoretical capacity, making it convenient for the reversible insertion/extraction of alkali metal ions.^[109] More importantly, MoS_2 can show either or both capacitive and pseudo-capacitive properties through surface redox reactions.^[88,120] However, the attractive force between layers of MoS_2 leads to serious aggregation, then resulting in the reduction on effective surface area and insufficient utilization of active sites.^[110,121] Moreover, the conversion reaction induced large structure change may cause pulverization of MoS_2 upon cycling, especially at high current densities.^[109,122]

Up to now, a lot of efforts have been devoted to the design of MoS_2 -based electrodes for SICs. To release the internal strain and ensure fast charge transfer, the design of open structure, increasing the interface spacing and coupling with carbonaceous substrate have been proved to be feasible for MoS_2 -based electrodes.^[110,111,123] In this regard, Qiu's group^[109] designed and synthesized MoS_2 nanoflowers with larger interlayer spacing supported on carbon fibers (E– MoS_2 /carbon fiber), and the typical fabrication process is shown in Figure 7a. The super wide interlayer spacing can not only decrease ion diffusion pathways and increase available active surface area, but also guarantee the rapid mass transfer. As a result, when coupling with AC to assemble the SIC, both high energy density and power density can be obtained owing to the high pseudocapacitive charge storage from the super wide interlayer spacing of E– MoS_2 /carbon fiber. Additionally, Li et al.^[110] synthesized the ultrathin MoS_2 nanosheet arrays vertically anchored on bagasse-derived three-dimensional porous carbon frameworks

(MoS_2 @BPC), as shown in Figure 7b. It should be noted that the BPC with porous structure can effectively improve the electrical conductivity, ion diffusion and structure stability of MoS_2 @BPC. When coupled with BPC (cathode), the hybrid capacitor (Figure 7c) can deliver both high energy density (112.2 Wh kg^{-1} at 55 W kg^{-1}) and power density (8333 W kg^{-1} at 53.2 Wh kg^{-1}), along with excellent cycling stability. Moreover, Wang et al.^[111] developed a SiO_2 -etching method for the synthesis of free-standing porous carbon nanofiber (PCNF) membrane with characteristic of flexible and light, which can be served as a scaffold for the in-situ growth of MoS_2 @poly(3,4-ethylenedioxothiophene) (PEDOT) nanosheets (Figure 7d). The resultant PCNF@ MoS_2 @PEDOT electrode demonstrates excellent sodium storage performance, including high specific capacity, good rate capability and robust long-term cycling stability. Furthermore, a quasi-solid-state SIC, using the PCNF@ MoS_2 @PEDOT as battery-type anode and AC as capacitive-type cathode, shows excellent electrochemical performances and a much low self-discharge rate as well as superior electrochemical performances. Table 4 shows the electrochemical performances of various metal sulfides as anode for SICs, from where we can see that the metal sulfides anodes coupled with porous cathodes can obtain both high energy density and power density.

3.2. Cathode Materials

As another important component of SICs, the cathode is designed to highly compatible with anion adsorption. At present, activated carbon, porous carbon and graphene are popular cathode materials for SICs. Generally, the capacitive-type electrode materials of SICs should have three properties: high specific surface area to obtain large capacitance; excellent intra- and interparticle conductivity and good electrolyte accessibility.^[28,29,128] Herein, the latest progress on cathode materials is summarized, especially focusing on the design of carbonaceous microstructure, regulation of specific surface

Table 4. Recent advances of SICs based on conversion-type anode materials.

Anode//Cathode	Electrolyte	Voltage window	Energy and power densities	Cycling performance	Year	Ref.
SnS_x/ZnS -reduced graphene oxide//porous carbon $\text{NiS}_x@\text{porous carbon matrix}/\text{AC}$	1 M NaClO_4 in EC/DMC	0–3.0 V	145.6 Wh kg^{-1} at 2250 W kg^{-1} 92.92 Wh kg^{-1} at 13500 W kg^{-1}	100% after 1000 cycles at 1.0 A g^{-1}	2021	[124]
	1 M NaClO_4 in EC/DEC with 5% FEC	1–4.0 V	99.3 Wh kg^{-1} at 140 W kg^{-1} 52.2 Wh kg^{-1} at 4480 W kg^{-1}	300 mA h g^{-1} after 800 cycles at 1.0 A g^{-1}	2020	[125]
MnS in N, S-doped carbon//N-doped carbon 3D inverse opal FeS quantum dots@NC//AC	1 M NaClO_4 in EC/DMC	0–4.0 V	139.8 Wh kg^{-1} at 230 W kg^{-1} 36.4 Wh kg^{-1} at 11500 W kg^{-1}	84.5% after 3000 cycles at 2.0 A g^{-1}	2020	[126]
	1 M NaClO_4 in EC/PC with 5% FEC	0.01–3.0 V	151.8 Wh kg^{-1} at 145 W kg^{-1}	91% after 5000 cycles at 1.0 A g^{-1}	2019	[127]
MoS ₂ /CoS ₂ /rGO//carbon cloth	1 M NaPF_6 in EC/DEC	0–3.0 V	153 Wh kg^{-1} at 562.5 W kg^{-1} 84.9 Wh kg^{-1} at 4500 W kg^{-1}	77% after 2000 cycles at 5 C	2019	[123]
MoS ₂ @bagasse-derived carbon//bagasse-derived porous carbon MoS ₂ -Carbon//porous carbon	1 M NaPF_6 in EC/PC	0–4.0 V	112.2 Wh kg^{-1} at 55 W kg^{-1} 53.2 Wh kg^{-1} at 8333 W kg^{-1}	90% after 1000 cycles at 2.0 A g^{-1}	2018	[110]
	1 M NaClO_4 in EC/DEC with 5% FEC	1.0–3.8 V	111.4 Wh kg^{-1} at 240 W kg^{-1} 19.1 Wh kg^{-1} at 12000 W kg^{-1}	77.3% after 10000 cycles at 2.0 A g^{-1}	2017	[122]

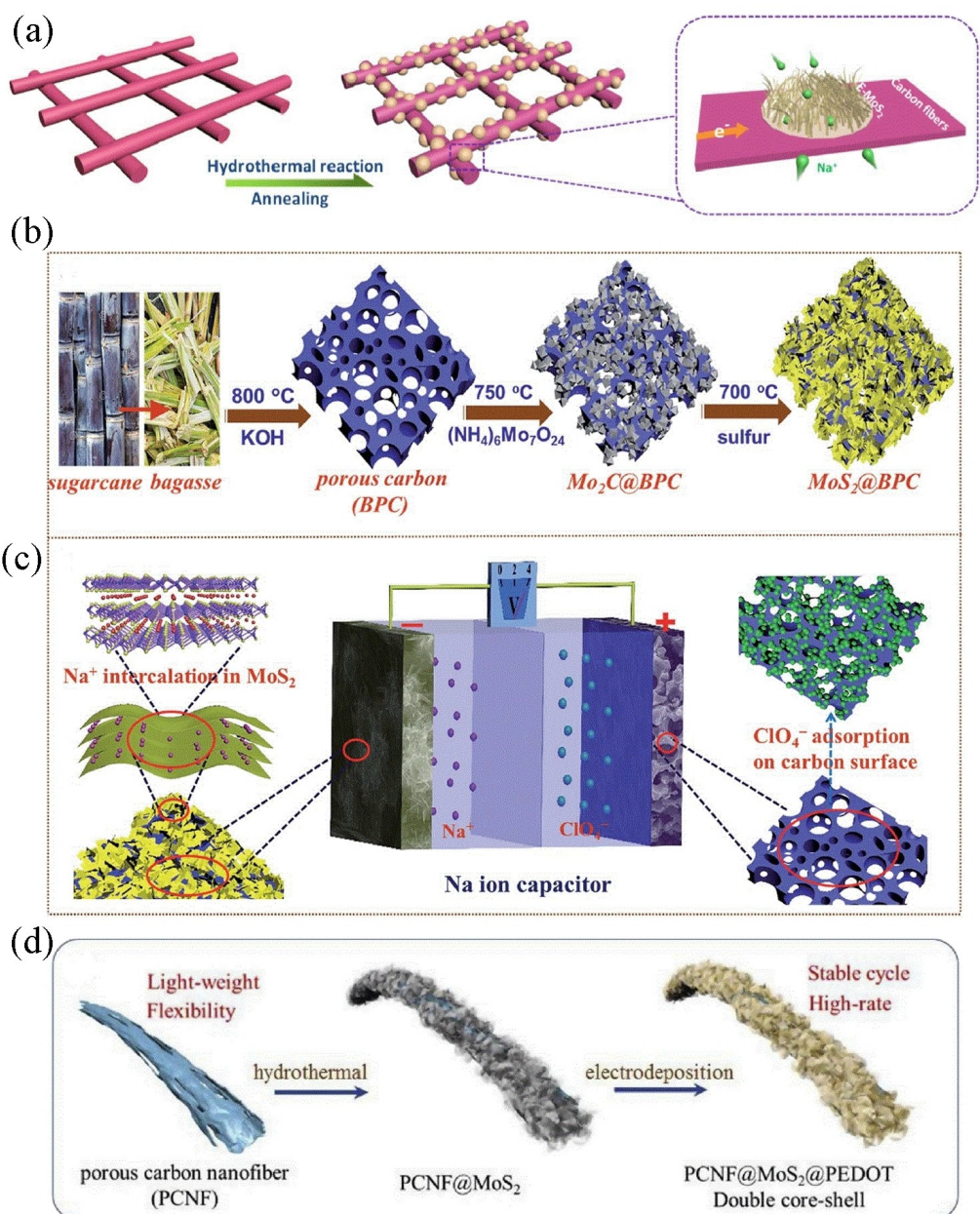


Figure 7. a) Schematic illustration of the preparation of MoS₂ nanoflowers with wide interlayer spacing on carbon fiber. Reproduced from Ref. [109] with permission. Copyright (2017) Elsevier Ltd. b) Illustration of the fabrication of MoS₂@bagasse derived porous carbon (MOS₂@BPC). c) The assembled SIC based on MoS₂@ BPC and BPC. Reproduced from Ref. [110] with permission. Copyright (2018) The Royal Society of Chemistry. d) Schematics of the synthetic route of flexible porous carbon nanofiber@MoS₂@ poly(3,4-ethylenedioxythiophene) electrode. Reproduced from Ref. [111] with permission. Copyright (2020) Elsevier B.V.

area/pore size/heteroatom doping and corresponding electrochemical performances.

3.2.1. Activated Carbon

Among all the available carbonaceous materials, ACs have attracted a lot of attention because of their porous structure, large surface area, low cost, corrosion resistance, low coefficient of expansion, non-toxicity and excellent physical/chemical properties, which renders ACs as the most suitable cathode for

SICs.^[67,129,130] Based on literature review of carbonaceous cathodes for SICs,^[131] specific surface area, pore size, carbonization degree play important roles for the electrochemical performances of ACs in SICs.

Biomass derived ACs with tunable specific surface area and pore size have become a research hotspot, and improved electrochemical performances are received through optimizing their morphology and structure.^[129] For example, Kiruthiga et al.^[80] reported the preparation of ACs using natural liquid honey as the starting material, and the carbonization process induces a high surface area of 1554 m² g⁻¹. Electrochemical test

coupled with a non-Faraday cathode demonstrates a high specific capacitance of 224 F g^{-1} . As known, large surface area of ACs can provide rich active sites for ion adsorption, and then high specific capacitance can be expected. In this regard, Nithya et al.^[130] reported a novel AC with a high specific surface area of $2042 \text{ m}^2 \text{ g}^{-1}$ derived from wool, which displays a higher specific capacitance of 256 F g^{-1} . After coupling with $\text{MoO}_2@r\text{GO}$ (anode), the hybrid device exhibits an energy density of 79 Wh kg^{-1} and a power density of 95 W kg^{-1} at the current density of 0.04 A g^{-1} as well as a capacity retention of 78% after 1000 cycles. The two examples shown above prove that the increase of specific surface area can indeed increase the specific capacitance of electrode and the corresponding SICs performances. However, the enhancement on electrochemical performance of SICs depends not only on the specific surface area, but also the pore size.

In general, the pores on the surface of ACs can be divided into three categories according to their diameter: I) micropores ($< 2 \text{ nm}$), II) mesopores ($2\text{--}50 \text{ nm}$) and III) macropores ($> 50 \text{ nm}$).^[5,51,132,133] Particularly, micropores when present in significant amounts can offer a high surface area to volume ratio, contributing to the adsorption/desorption processes.^[134\text{--}136] In regard of mesopores, both large surface area and high adsorbate accessibility through rich transport channels can be obtained simultaneously.^[29] The study of Biswal et al.^[137] showed that the presence of micropores and mesopores on the surface of ACs can not only contribute to the increase of specific surface area, but also provide transport channels for the mass transfer, leading to improved electrochemical performance of SICs. Electrode materials with three-dimensional interpenetrated structures, especially interconnected macropores networks, can largely improve the penetration of electrolyte in the electrode materials. Sun et al.^[138] created three-dimensional interpenetrated carbonaceous materials with rich macropores through a template-free method, employing yeast cells as the starting materials. The resultant materials showed high surface area as well as superior electrochemical performances.

3.2.2. Graphene and Carbon Nanotube

Compared with ACs featuring amorphous structure, low electrical conductivity and power density, graphene and carbon nanotubes (CNTs) with high degree of crystallinity possess high electronic conductivity, which is of significant importance for improving their electrochemical performances.^[86,139,140] However, the serious aggregation of graphene due to the large surface tension and low surface area of CNTs restrict their applications.^[133,139] Previous studies have demonstrated that the rational combination of CNTs with ACs or graphene can not only take full advantage of the high conductivity of CNTs, but also the high surface areas of ACs or graphene, which then contributes to improved electrochemical performance.^[138,139]

Different with the CNTs possessing a tubular structure, graphene, a typical two-dimensional nanostructure, features ultrahigh specific surface area ($> 2600 \text{ m}^2 \text{ g}^{-1}$), superior in-plane

conductivity and large layer spacing, has shown excellent performances in various energy devices.^[29,62] To mitigate the aggregation of graphene, reducing the graphene oxide (GO) into reduced graphene oxide (rGO) through thermal or chemical reduction is one of the most popular approach.^[141] The porous structure, combining the abundant pores and large interlayer spacing, can offer a conductive network for the diffusion of ions and charge transfer, and excellent electrochemical performance can be expected when employed as capacitive cathode in hybrid devices.^[142] For instance, Lv's group^[133] prepared a nitrogen, boron co-doped expanded rGO (NBEG) and polyimide/graphene oxide derived carbon (PIGC). The typical fabrications of NBEG and PIGC are shown in Figure 8a, and the corresponding SEM images of NBEG and PIGC are shown in Figure 8b and 8c. The heteroatom-doping endows the NBEG with a high specific capacitance of 328 F g^{-1} . Figure 8d illustrates the charge/discharge profiles of the PIGC//NBEG hybrid device within $0\text{--}4.2 \text{ V}$, which maintains an ideal symmetry shape at all current densities, thereby demonstrating its excellent electrochemical reversibility. Besides, the comparison on energy/power densities indicates that PIGC//NBEG possesses higher energy density and power density than those of PIGC//AC (Figure 8e). Moreover, the cycling stability of the PIGC//NBEG is also confirmed through the long-term test (Figure 8f). The excellent performance can be ascribed to the enhanced rate capability of PIGC and high specific capacitance of NBEG as well as the balance on both capacity and kinetics between cathode and anode. Besides, a quasi-solid-state SIC, employing surface oxygen-functionalized crumpled graphene (OCG) as both anode and cathode electrodes and a gel polymer as the electrolyte, can achieve a high energy density of 121.3 Wh kg^{-1} , a high power density of 8000 W kg^{-1} and a robust long-term cycling stability over 2500 cycles with a capacitance retention of 86.7%.^[139] Such high SIC performance should be mainly ascribed to the elaborate design of electrode and device configuration.^[143,144] Table 5 illustrates the recent advances on the carbonaceous cathodes for SICs, which emphasizes the importance of fabrication porous structure with high specific surface to improve the electrochemical performance of SICs.

3.2.3. Other Materials

In addition to the cathode materials described above, there are still many other types of materials that are suitable as cathodes for SICs. MXene-based materials have now attracted the attention as candidates for energy storage owing to the spontaneous intercalation of variety of cations between their layers.^[77] The studies on $\text{Ti}_3\text{C}_2\text{T}_x$ and Ti_2CT_x have demonstrated their excellent performances as anode materials for SICs due to their operating potential window.^[25,81] V_2CT_x MXene, with a potential window ranging from 1.0 to 3.5 V, shows promise as cathode material for SICs.^[144] Dall'Agnese and his co-workers^[144] assembled a full cell with hard carbon as the anode and V_2CT_x as the cathode, which manifests a maximum voltage of 3.5 V, along with a capacity of 50 mAh g^{-1} . Detailed investigations

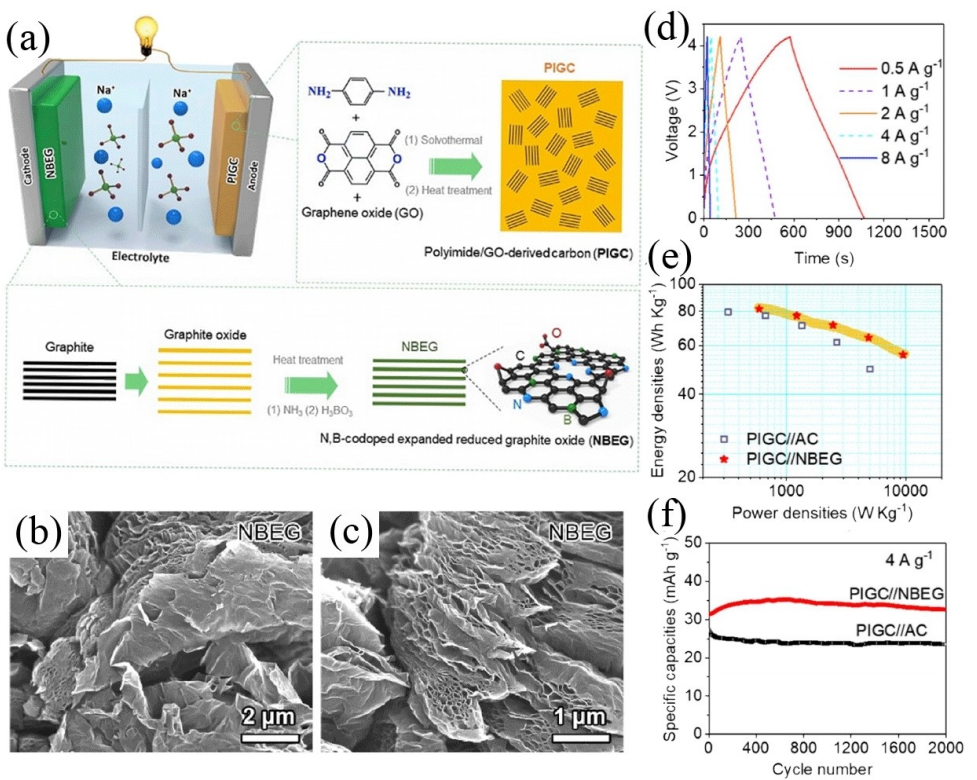


Figure 8. a) Illustration of the SIC and the preparation process of polyimide/GO derived carbon (PIGC) and N, B-doped reduced graphite oxide (NBEG). b, c) SEM images of NBEG. Electrochemical tests of the PIGC//NBEG: d) galvanostatic charge/discharge curves, e) energy-power properties, and f) cycling performance at 4.0 A g^{-1} . Reproduced from Ref. [133] with permission. Copyright (2020) Chinese Materials Research Society.

Table 5. Table. 5 A summary of recent advances on SICs based on carbonaceous cathodes.

Cathode//Anode	Electrolyte	Specific surface area of cathode	Energy and power densities	Cycling performance	Year	Ref.
Activated carbon nanofiber//CNTs@N, O-carbon nanofiber	1 M NaClO ₄ in EC/PC/FEC	1963 m ² g ⁻¹	59.2 Wh kg ⁻¹ at 275 W kg ⁻¹	48.6% after 5000 cycles at 0.5 A g^{-1}	2020	[145]
Nitrogen-doped hierarchical porous activated carbon//N-doped 3D carbon	1 M NaClO ₄ in EC/EMC/DMC	1478 m ² g ⁻¹	38.7 Wh kg ⁻¹ at 5500 W kg ⁻¹ 115.0 Wh kg ⁻¹ at 200 W kg ⁻¹			
Garlic derived porous carbon//garlic derived hard carbon	1 M NaClO ₄ in EC/PC/FEC	1682 m ² g ⁻¹	156.0 Wh kg ⁻¹ at 355 W kg ⁻¹ 31.0 Wh kg ⁻¹ at 38910 W kg ⁻¹	73% after 10000 cycles at 5.0 A g^{-1}	2019	[67]
N, O-doped hierarchical porous carbon//N, O-doped hierarchical porous carbon	1 M NaClO ₄ in EC/PC/FEC	3285 m ² g ⁻¹	22.3 Wh kg ⁻¹ at 15900 W kg ⁻¹	81% after 2500 cycles at 3.5 A g^{-1}	2019	[129]
N-doped hierarchical porous carbon//TiO _x N _y /C	1 M NaClO ₄ in EC/DEC/FEC	—	103.2 Wh kg ⁻¹ at 70 W kg ⁻¹ 80.0 Wh kg ⁻¹ at 4000 W kg ⁻¹	95% after 5000 cycles at 1.0 A g^{-1}	2018	[131]
3D nanoporous carbon//TiO ₂ /C	1 M NaClO ₄ in EC/PC/FEC	3738 m ² g ⁻¹	142.7 Wh kg ⁻¹ at 25000 W kg ⁻¹	90% after 10000 cycles at 1.0 A g^{-1}	2018	[85]
Biomass derived activated carbon//MoO ₂ @rGO	0.75 M NaPF ₆ in EC/DEC	2042 m ² g ⁻¹	79.0 Wh kg ⁻¹ at 95 W kg ⁻¹	78% after 1000 cycles at 0.04 A g^{-1}	2018	[130]
Honey derived activated carbon//V ₂ O ₅ @rGO	0.75 M NaPF ₆ in EC/DEC	1554 m ² g ⁻¹	65.0 Wh kg ⁻¹ at 72 W kg ⁻¹	74% after 1000 cycles at 0.06 A g^{-1}	2017	[146]

show that both pseudocapacitive and diffusion dominated electrochemical process happened in the potential range. As an intermediate material between polymer and carbon, pyropolymer can be obtained through pyrolyzing a polymer precursor at low temperature ($<1000^\circ\text{C}$), and the received hexagonal carbon are rich in heteroatoms and defects, leading to high electrochemical performance.^[147] In view of this, Jin et al.^[147]

reported a hierarchically nanoporous pyropolymer nanofibers (HN-PNFs) through a combined approach containing electro-spinning and thermal treatment with KOH. The high surface area ($3950.7 \text{ m}^2 \text{ g}^{-1}$) and numerous redox-active heteroatoms (O and N) endow the HN-PNFs with high sodium storage activity. A hybrid device, employing PNFs and HN-PNFs as anode and cathode, shows a high specific energy density of

258 Wh kg⁻¹ at 245 W kg⁻¹ and power density of 21500 W kg⁻¹ at 78 Wh kg⁻¹, along with a superior cycling stability over 2000 cycles.

Manganese, as a transition metal element, has attracted a lot of attention in the field of energy storage due to its stable oxidation state, tuned morphology/structure and pseudocapacitive feature, which shows outstanding performances in SCs.^[141,149,150] As for SICs, Na_{0.44}MnO₂ with large tunnels shows potential as high-performance cathode for SICs.^[139] Xie et al.^[139] reported a new-type SIC assembled with Ti₃C₂T_x MXene/CNT (anode) and Na_{0.44}MnO₂ (cathode), which can achieve a high volumetric capacity of 286 mAh cm⁻³. Besides, Na₃V₂(PO₄)₃ (NVP), featuring Na⁺ superionic conductor, has been proved to be high-performance cathode material for SIBs, which originates from its open structure as well as its multistep redox reactions.^[148,151] To further improve the electrochemical performance of NVP, the introduction of carbonaceous agent appears to be the one of the most efficient approach.^[148] Recently, the interest on the utilization of NVP as cathode material for SICs has grown. For instance, Fan et al.^[148] reported the combination of NVP with metal organic framework array derived N-doped mesoporous carbon nanosheets (mp-CNSs) on carbon fiber cloth (CFC), and similar approach was employed for the synthesis of VO₂@mp-CNSs/CFC. Figure 9a shows the SIC device based on NVP@mp-CNSs/CFC and

VO₂@mp-CNSs/CFC. Due to the rational material design endowed structure advantages, the diffusion of Na⁺ in the two electrodes is greatly improved, as shown in Figure 9b and c, leading to excellent rate capability. Figure 9d and e depict the long-term cycling performance at 1.0 A g⁻¹ and Ragone plots of the as-assembled hybrid device, highlighting its superior electrochemical performances. Specifically, the flexible SIC can deliver both high energy density and power density as well as well superior cycling stability (78% capacity retention after 2000 cycles at 1.0 A g⁻¹). In principle, the introduction of mp-CNSs into the cathode and anode can largely alleviate their mismatching on both capacity and kinetics, thereby leading to rapid charge transfer.^[152] Moreover, more information on the novel cathode materials for the SICs has been listed in Table 6, which manifests both high energy density and power density.

4. SICs Based on Dual Carbon

To date, although the electrochemical performances of SICs based on carbonaceous cathodes and various types of anodes have been extensively reported, and improved electrochemical performances have been indeed received, they still suffer from low power density and limited cycling life, which should be mainly ascribed to the inevitable difference in structural

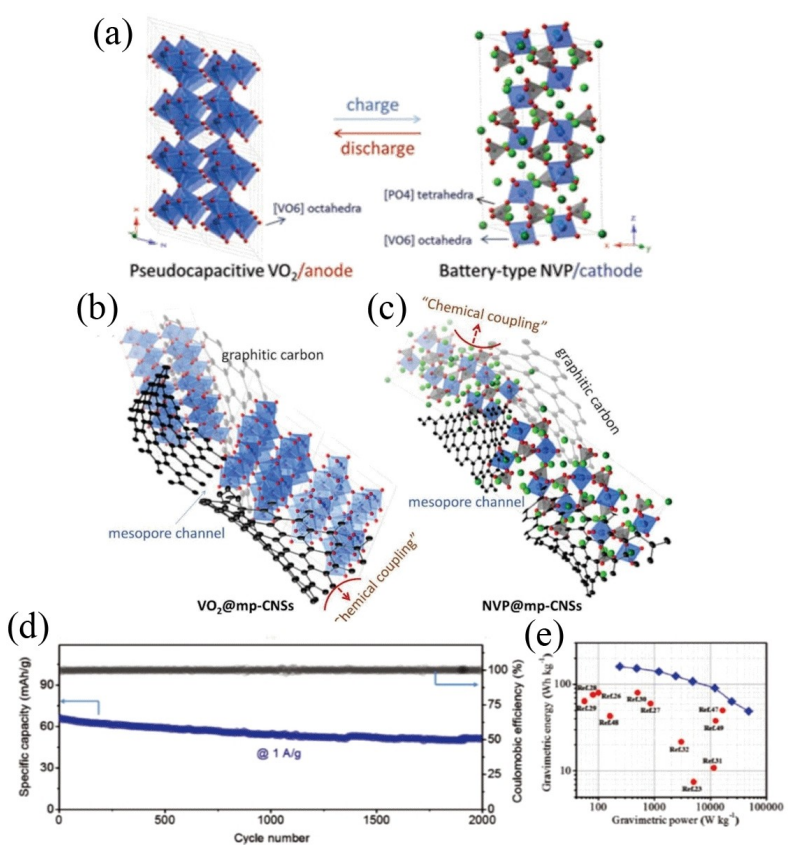


Figure 9. a) Illustration of SIC device based on NVP@N-doped mesoporous carbon nanosheet/carbon fiber cloth (NVP@mp-CNSs/CFC) and VO₂@mp-CNSs/CFC and high-rate sodium storage in these two electrodes (b and c). d) Cycling performance at 1.0 A g⁻¹ and e) Ragone plots of the SIC. Reproduced from Ref. [148] with permission. Copyright (2018) Wiley-VCH.

Table 6. A summary of recent advances of SICs based on novel cathode materials.

Cathode//Anode	Electrolyte	Potential range	Energy and power densities	Cycling performance	Year	Ref.
Na ₃ (VO) ₂ (PO ₄) ₂ F@CNF//porous carbon nanofibers	1 M NaClO ₄ in EC/DEC	1–4.0 V	182.8 Wh kg ⁻¹ at 15898 W kg ⁻¹	92 % after 1000 cycles at 10 C	2020	[153]
Na _{0.5} Mn _{0.5} Co _{0.48} Mg _{0.02} O ₂ //AC	1 M NaClO ₄ in PC	0–3.0 V	34.0 Wh kg ⁻¹ at 150 W kg ⁻¹	72 % after 3000 cycles at 1.0 A g ⁻¹	2020	[150]
P ₂ –Na _{0.67} Co _{0.5} Mn _{0.5} O ₂ //ZIF-8 derived carbon	1 M NaClO ₄ in EC/PC	0–3.0 V	18.8 Wh kg ⁻¹ at 12750 W kg ⁻¹	92 % after 2000 cycles at 5.0 A g ⁻¹	2018	[154]
Na _{0.66} Mn _{0.54} Ni _{0.13} Co _{0.13} O ₂ @Al ₂ O ₃ //AC	1 M NaClO ₄ in EC/DEC	0–3.0 V	63.0 Wh kg ⁻¹ at 6600 W kg ⁻¹	98 % after 10000 cycles at 0.35 A g ⁻¹	2018	[155]
Na _{0.4} MnO ₂ //AC	1 M NaClO ₄ in PC	0–2.7 V	17.4 Wh kg ⁻¹ at 67 W kg ⁻¹ 0.8 Wh kg ⁻¹ at 4750 W kg ⁻¹	85 % after 1000 cycles at 39 C	2018	[156]

stability between the metal-based anodes and carbonaceous cathodes.^[29,141] Due to the large volume expansion and electrochemical instability of the metal-based electrodes as well as the mismatch on dynamics between anode/cathode, the charge/discharge rate, cycling stability and reliability of the hybrid device will be affected.^[142] In this regard, many researchers recently have turned their attention to the fabrication of all-carbon based SICs.^[28] Besides, the “homologous strategy” has been widely employed to construct suitable carbonaceous anode and cathode materials for high-performance SICs.^[66] The carbonaceous anode and cathode materials prepared from the same precursor possess similar micro-structure with amorphous feature.^[73] Moreover, SICs assembled with electrodes from the same precursor manifest low tortuosity compared with devices constructed by electrodes prepared from different precursors, which can promote the charge transfer and ion diffusion.^[157] Specifically, some studies on SICs based on all-carbon electrodes have been introduced in the sections of Anode Material and Cathode Materials due to their excellent electrochemical performances.^[68,158] This section focuses on the detailed explanations on the improved electrochemical performance of all-carbon based SICs.

To mitigate the kinetics mismatching and assemble all-carbon based SICs, Jian and his co-worker^[134] prepared a bio-waste pine cone shell derived carbon nanosheets (PSCSs) and a carbonaceous cathode derived from covalent triazine framework (OPDN-CTF-A). The SIC assembled with the two carbonaceous materials can achieve both high energy density (111 Wh kg⁻¹) and power output (14200 W kg⁻¹) as well as ultra-stable cycling (90.7% capacity retention after 10000 cycles). Basically, the high performance of OPDN-CTF-A/PSCSs device can be attributed to the following reasons: I) facilitated sodiation process in the large interlayer spacing of PSCSs; II) high pseudocapacitance from the OPDN-CTF-A with high surface area and hierarchical pores; III) improved matching on kinetics and enhanced electronical conductivity of the all-carbon electrodes.^[66,67] The above example shows that SIC based on two different carbonaceous materials with features suitable for anode and cathode can obtain high electrochemical performance. In view of this, cathode and anode materials derived from the same starting material through structure engineering are believed to further improve the SICs performances. Yan and his co-worker^[56] presented a simple method to prepare three-dimensional framework carbon

(3DFC) and 3DFC derived nanoporous carbon (3DFAC), which can be employed as battery-type anode and capacitive-type cathode, respectively, as shown in Figure 10a. The assembled SIC based on 3DFC and 3DFAC with anode/cathode mass ratio of 1:2 displays the highest capacity values at various current densities, and shows the highest energy density of 111 Wh kg⁻¹ (at power density of 200 W kg⁻¹). Besides, this device can deliver an impressive power density of 20000 W kg⁻¹ at a high energy density of 67 Wh kg⁻¹, along with long cycling stability up to 15000 cycles (Figure 10b). Such remarkable performance of 3DFC//3DFAC originates from the structure advantages of the electrode materials employed, from where the 3D architecture and large graphitic interlayer spacing of 3DFC can facilitate the insertion/extraction of Na⁺ and high surface area and rich pores of 3DFAC can provide abundant adsorption sites, thus contributing to the high electrochemical performances.^[63] Similarly, Yan’s group^[52] constructed anode and cathode materials with similar pore microstructure using bacterial cellulose as the starting material. Due to the homologous strategy, the products show typical hierarchical micropore-mesopore networks with pore size distribution of 1–3 nm, which endows the samples with fast charge transfer and rapid ion diffusion. Generally, the anode material was obtained after pyrolysis of 2, 2, 6, 6-tetramethylpiperidine-1-oxyl modified bacterial cellulose, and the cathode material was received through KOH activation of the anode materials, as illustrated in Figure 11a. Beside, the optimized mass ratio (1:1) between cathode and anode results in both high energy density and power density as well as robust cycling stability (Figure 11b–c). Specifically, the fabricated SIC delivers a high energy density of 124 Wh kg⁻¹ at a power density of 210 W kg⁻¹ and a power density of 15500 W kg⁻¹ at an energy density of 22 Wh kg⁻¹ within a potential range of 0–4.2 V. Furthermore, Ji and co-worker^[53] demonstrated a novel SIC based on nitrogen-doped 3D carbon (NHPC, anode) and nitrogen-doped hierarchical porous activated carbon (NHPAC, cathode) derived from the NHPC. The NHPC displays a high reversible specific capacity of 197 mAh g⁻¹ at 2.0 A g⁻¹, and the strong pseudocapacitive storage induced quickly physical adsorption/desorption of Na⁺ contributes to the high sodium storage performances. As for the NHPAC cathode, its large specific surface area of 1478 m² g⁻¹ with abundant meso/macropores can enable fast adsorption/desorption of anions on its surface.^[158] These structure features endow the NHPC//NHPAC device with a high

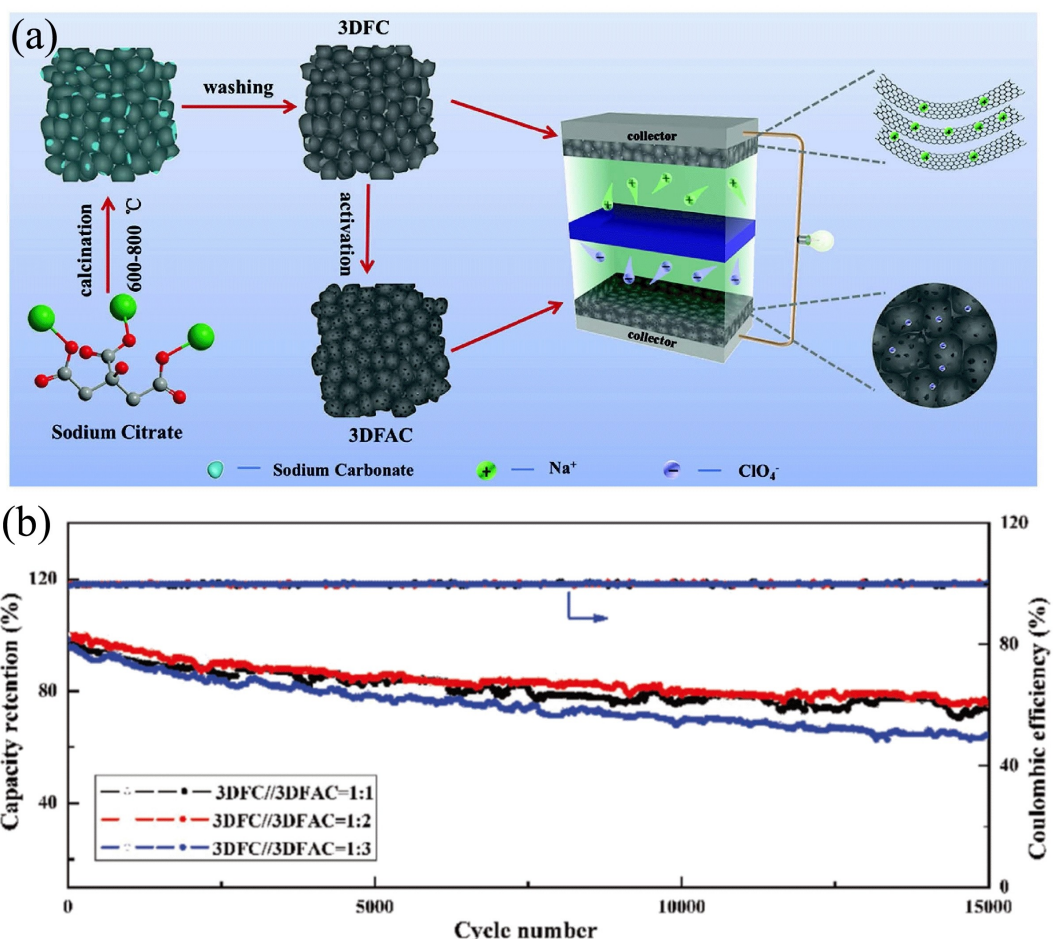


Figure 10. a) Illustration of the preparation of 3D framework carbon (3DFC) and 3D framework nanoporous carbon (3DFAC) from the same raw material and the construction of dual-carbon SIC based on the battery-type 3DFC and capacitive-type 3DFAC cathode. b) Cycling stability of 3DFC//3DFAC with different mass ratios, tested at 2.0 A g⁻¹ for 15000 cycles ranging from 0 to 4.0 V. Reproduced from Ref. [56] with permission. Copyright (2018) Wiley-VCH.

energy density of 115 Wh kg⁻¹ at 200 W kg⁻¹ as well as long-term cyclability ranging from 0 to 4.0 V. Table 7 lists the recent advances on the dual carbon-based SICs. Due to the well-matched kinetics and capacity, excellent electrochemical performances have been obtained.

5. Conclusions and Outlook

In summary, SICs are expected to play important roles in the field of energy storage devices due to their advantages of resource abundance, high energy density and power density. From the material point of view, electrode material is the most

Table 7. A summary of recent advances of SICs based on dual-carbon electrodes.

Anode//Cathode	Electrolyte	Voltage window	Energy and power densities	Cycling performance	Year	Ref.
3D N, S co-doped porous carbon nanosheet//hierarchically porous carbon	1 M NaClO ₄ in EC/DMC	0–4.0 V	199 Wh kg ⁻¹ at 200 W kg ⁻¹ 53 Wh kg ⁻¹ at 20000 W kg ⁻¹	82% after 8000 cycles at 5.0 A g ⁻¹	2020	[159]
N functionalized carbon nanocages//N functionalized carbon nanocages	1 M NaClO ₄ in EC/DEC	2.7–4.2 V	102.5 Wh kg ⁻¹ at 331 W kg ⁻¹ 40.3 Wh kg ⁻¹ at 12692 W kg ⁻¹	74.2% after 100000 cycles at 50.0 A g ⁻¹	2019	[160]
Nanoporous hard carbon//N-doped carbon	1 M NaClO ₄ in EC/DMC	1.3–4.2 V	181 Wh kg ⁻¹ at 250 W kg ⁻¹	–	2019	[157]
N doped carbon//porous carbon	1 M NaClO ₄ in DC/DEC	0–4.0 V	37 Wh kg ⁻¹ at 110 W kg ⁻¹	85 % after 10000 cycles at 5.0 A g ⁻¹	2018	[68]
Three-dimensional carbon framework//sodium alginate derived activated carbon	1 M NaClO ₄ in EC/DMC	0–4.0 V	133.2 Wh kg ⁻¹ at 200 W kg ⁻¹ 44 Wh kg ⁻¹ at 20000 W kg ⁻¹	86% after 4000 cycles at 2.0 A g ⁻¹	2018	[54]
Fruits derived carbon microspheres//Fruits derived AC	1 M NaClO ₄ in EC/DEC	2.0–4.0 V	52.2 Wh kg ⁻¹ at 300 W kg ⁻¹	85.7% after 2000 cycles at 2.0 A g ⁻¹	2017	[158]
3D framework carbon//3DFC-derived nanoporous carbon	1 M NaClO ₄ in EC/DMC	0–4.0 V	110 Wh kg ⁻¹ at 200 W kg ⁻¹ 67 Wh kg ⁻¹ at 20000 W kg ⁻¹	80% after 10000 cycles at 2.0 A g ⁻¹	2017	[56]

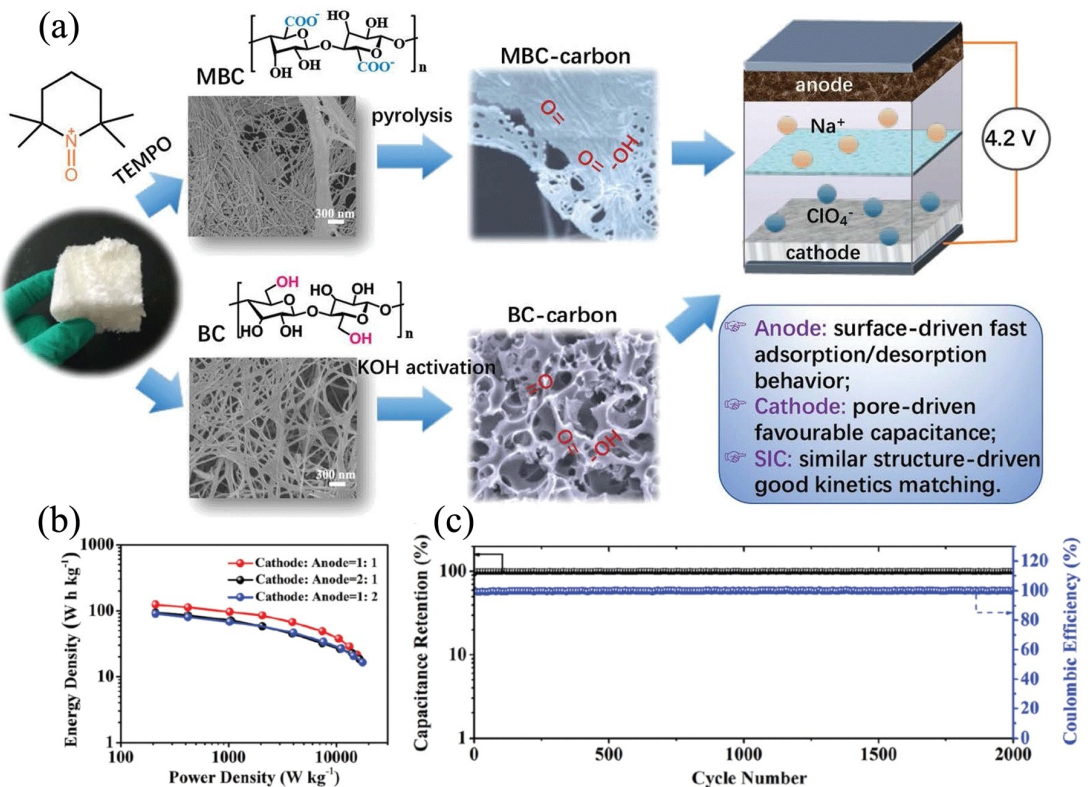


Figure 11. a) Material synthesis process of the anode and cathode materials derived from bacterial cellulose and the corresponding charge storage mechanism in SICs. b) Comparison of energy density and power density of the assembled SICs with various mass ratios. c) Cycling performance of the assembled SIC at 1.0 A g^{-1} with the mass ratio of 1:1 between cathode to anode. Reproduced from Ref. [52] with permission. Copyright (2020) The Royal Society of Chemistry.

important component in SICs, directly affecting the energy density, power density and cycling life. This review summarizes the latest developments in electrode materials for SICs, especially focusing on the relationship between the electrode structure and corresponding electrochemical performances. Figure 12 illustrates the guidance for the materials design of both anode and cathode for SICs, combining the above introductions on anode materials, cathode materials and the dual-carbon based SICs, from where it can be seen that the smart design for both cathode and anode materials as well as their rational coupling have significant effect on electrochemical performances of assembled SICs. Although much improved electrochemical performances of SICs have been reported, the sluggish diffusion kinetics of Na⁺ upon cycling as well as the mismatching on capacity/kinetics between cathode and anode is still challenging. Therefore, the research emphasis of SICs should be put in the following aspects.

I) Despite various anode materials with different mechanisms have been employed in SICs, the electrochemical performances on sodium storage are still unsatisfied. To alleviate the kinetics mismatching, exploring new-type anode materials with suitable channels for Na⁺ diffusion and excellent electronic conductivity to accelerate the charge transfer is of significant importance to further improve the electrochemical performance of SICs.

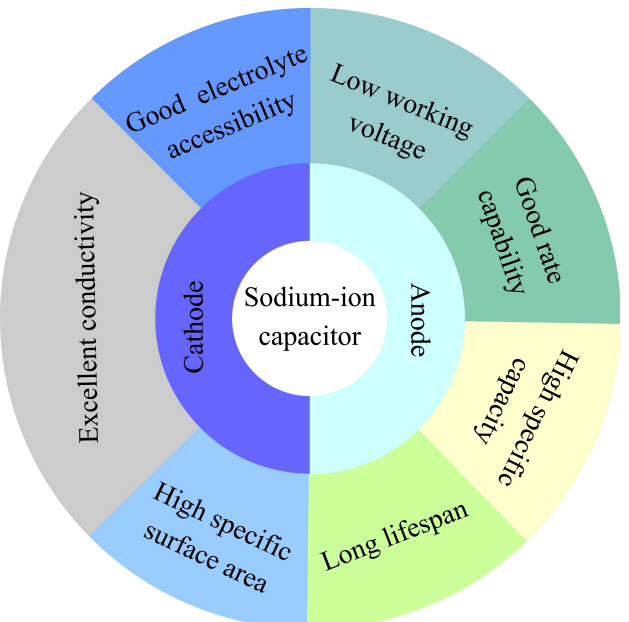


Figure 12. Illustration of design on electrode materials to improve the electrochemical performance of SICs.

II) ACs with high surface areas have been widely used as cathode for SICs, but suffer from low power density, further leading to mismatching on kinetics/capacity with the anodes.

In this regard, novel cathode materials beyond ACs are extremely urgent. Besides, developing novel method to fabricate carbonaceous cathode with controllable pore size, high specific surface area and good electrolyte accessibility are desired. Moreover, taking effort on the biomass derived carbonaceous cathodes can not only decrease the fabrication cost but also promote the recycling of waste.

III) Except the electrode materials, electrolytes also play important roles for the practical performance of SICs. Ionic liquid electrolyte with high voltage and high safety is promising to increase the energy density of the SICs. Besides, flexible SICs based on gel electrolyte is also attracting increasing attention due to their wide applications in future. What's more, theory calculation should be employed in the design of electrode materials, providing guidance for their synthesis and solid evidence for the improved electrochemical performances.

Acknowledgements

The authors acknowledge the financial support from National Natural Science Foundation of China (21978251) and a project funded by the Priority Academic Program Development of Jiangsu Higher Education Institutions.

Conflict of Interest

The authors declare no conflict of interest.

Keywords: sodium-ion hybrid capacitor · electrode materials · energy-power density · cycling stability

- [1] J. Ding, W. Hu, E. Paek, D. Mitlin, *Chem. Rev.* **2018**, *118*, 6457–6498.
- [2] M. Arnaiz, D. Shannukaraj, D. Carriazo, D. Bhattacharjya, A. Villaverde, M. Armand, J. Ajuria, *Energy Environ. Sci.* **2020**, *13*, 2441–2449.
- [3] B. Wen, Z. Deng, P.-C. Tsai, Z. W. Lebens-Higgins, L. F. J. Piper, S. P. Ong, Y.-M. Chiang, *Nat. Energy* **2020**, *5*, 578–586.
- [4] R. Hou, B. Liu, Y. Sun, L. Liu, J. Meng, M. D. Levi, H. Ji, X. Yan, *Nano Energy* **2020**, *72*, 104728.
- [5] M. Arnaiz, P. Huang, J. Ajuria, T. Rojo, E. Goikolea, A. Balducci, *Batteries & Supercaps* **2018**, *1*, 204–208.
- [6] T. Nakamura, K. Chiba, M. Fakkao, Y. Kimura, K. Nitta, Y. Terada, Y. Uchimoto, K. Amezawa, *Batteries & Supercaps* **2019**, *2*, 688–694.
- [7] D. Yan, J. Zhang, D. Xiong, S. Huang, J. Hu, M. E. Pam, D. Fang, Y. Wang, Y. Shi, H. Y. Yang, *J. Mater. Chem. A* **2020**, *8*, 11529–11537.
- [8] B. Anothumakkool, S. Wiemers-Meyer, D. Guyomard, M. Winter, T. Brousse, J. Gaubicher, *Adv. Energy Mater.* **2019**, *9*, 1900078.
- [9] Y. Ma, H. Chang, M. Zhang, Y. Chen, *Adv. Mater.* **2015**, *27*, 5296–5308.
- [10] W. Zuo, R. Li, C. Zhou, Y. Li, J. Xia, J. Liu, *Adv. Sci.* **2017**, *4*, 1600539.
- [11] T. Liu, Y. Zhang, C. Chen, Z. Lin, S. Zhang, J. Lu, *Nat. Commun.* **2019**, *10*, 1965.
- [12] K. Li, J. Zhang, D. Lin, D. W. Wang, B. Li, W. Lv, S. Sun, Y. B. He, F. Kang, Q. H. Yang, L. Zhou, T. Y. Zhang, *Nat. Commun.* **2019**, *10*, 725.
- [13] C. Zhao, Q. Wang, Z. Yao, J. Wang, B. Sánchez-Lengeling, F. Ding, X. Qi, Y. Lu, X. Bai, B. Li, H. Li, A. Aspuru-Guzik, X. Huang, C. Delmas, M. Wagemaker, L. Chen, Y.-S. Hu, *Science* **2020**, *370*, 708–711.
- [14] Z. Hu, L. Wang, K. Zhang, J. Wang, F. Cheng, Z. Tao, J. Chen, *Angew. Chem. Int. Ed.* **2014**, *126*, 13008–13012.
- [15] J. Huang, X. Guo, X. Du, X. Lin, J.-Q. Huang, H. Tan, Y. Zhu, B. Zhang, *Energy Environ. Sci.* **2019**, *12*, 1550–1557.
- [16] X. Zhao, Y. Zhang, Y. Wang, H. Wei, *Batteries & Supercaps* **2019**, *2*, 899–917.
- [17] G. G. Amatucci, F. Badway, A. D. Pasquier, T. Zheng, *J. Electrochem. Soc.* **2001**, *148*, A930–A939.
- [18] K. Kuratani, M. Yao, H. Senoh, N. Takeichi, T. Sakai, T. Kiyobayashi, *Electrochim. Acta* **2012**, *76*, 320–325.
- [19] Z. Hu, Z. Zhu, F. Cheng, K. Zhang, J. Wang, C. Chen, J. Chen, *Energy Environ. Sci.* **2015**, *8*, 1309–1316.
- [20] Y. Jin, Y. Xu, P. M. L. Le, T. D. Vo, Q. Zhou, X. Qi, M. H. Engelhard, B. E. Matthews, H. Jia, Z. Nie, C. Niu, C. Wang, Y. Hu, H. Pan, J.-G. Zhang, *ACS Energy Lett.* **2020**, *5*, 3212–3220.
- [21] W. Li, R. Fang, Y. Xia, W. Zhang, X. Wang, X. Xia, J. Tu, *Batteries & Supercaps* **2019**, *2*, 9–36.
- [22] Q. Liu, D. Mu, B. Wu, L. Wang, L. Gai, F. Wu, *ChemSusChem* **2017**, *10*, 786–796.
- [23] Z. Huang, A. Chen, F. Mo, G. Liang, X. Li, Q. Yang, Y. Guo, Z. Chen, Q. Li, B. Dong, C. Zhi, *Adv. Energy Mater.* **2020**, *10*, 2001024.
- [24] Y. Zhang, J. Jiang, Y. An, L. Wu, H. Dou, J. Zhang, Y. Zhang, S. Wu, M. Dong, X. Zhang, Z. Guo, *ChemSusChem* **2020**, *13*, 2522–2539.
- [25] X. Wang, S. Kajiyama, H. Iinuma, E. Hosono, S. Oro, I. Moriguchi, M. Okubo, A. Yamada, *Nat. Commun.* **2015**, *6*, 6544.
- [26] Y. Fang, L. Xiao, J. Qian, Y. Cao, X. Ai, Y. Huang, H. Yang, *Adv. Energy Mater.* **2016**, *6*, 1502197.
- [27] J. Ajuria, E. Redondo, M. Arnaiz, R. Mysyk, T. Rojo, E. Goikolea, *J. Power Sources* **2017**, *359*, 17–26.
- [28] B. Wang, X. Gao, L. Xu, K. Zou, P. Cai, X. Deng, L. Yang, H. Hou, G. Zou, X. Ji, *Batteries & Supercaps* **2021**, *4*, 538–553.
- [29] F. Li, Z. Zhou, *Small* **2018**, *14*, 1701961.
- [30] Z. Xu, H. Fu, K. Yao, X. Shen, Z. Li, L. Fu, J. Huang, J. Li, *Batteries & Supercaps* **2018**, *1*, 184–191.
- [31] H. Wu, X. Li, L. Chen, Y. Dan, *Batteries & Supercaps* **2019**, *2*, 144–152.
- [32] A. M. Navarro-Suárez, K. Maleski, T. Makaryan, J. Yan, B. Anasori, Y. Gogotsi, *Batteries & Supercaps* **2018**, *1*, 33–38.
- [33] M. Mokhlesur Rahman, M. Zhou, I. Sultana, S. Mateti, A. Falin, L. H. Li, Z.-S. Wu, Y. Chen, *Batteries & Supercaps* **2019**, *2*, 160–167.
- [34] J. Li, Z. Ding, J. Li, C. Wang, L. Pan, G. Wang, *Chem. Eng. J.* **2021**, *407*, 127199.
- [35] J. Li, D. Yan, T. Lu, Y. Yao, L. Pan, *Chem. Eng. J.* **2017**, *325*, 14–24.
- [36] J. Li, J. Li, D. Yan, S. Hou, X. Xu, T. Lu, Y. Yao, W. Mai, L. Pan, *J. Mater. Chem. A* **2018**, *6*, 6595–6605.
- [37] J. Li, D. Yan, S. Hou, Y. Li, T. Lu, Y. Yao, L. Pan, *J. Mater. Chem. A* **2018**, *6*, 1234–1243.
- [38] J. Li, D. Yan, X. Zhang, S. Hou, T. Lu, Y. Yao, L. Pan, *J. Mater. Chem. A* **2017**, *5*, 20428–20438.
- [39] J. Li, Z. Ding, L. Pan, J. Li, C. Wang, G. Wang, *Carbon* **2021**, *173*, 31–40.
- [40] H. Ji, T. Wang, Y. Liu, C. Lu, G. Yang, W. Ding, W. Hou, *Chem. Commun.* **2016**, *52*, 12725–12728.
- [41] M. Chen, X. Shen, K. Chen, Q. Wu, P. Zhang, X. Zhang, G. Diao, *Electrochim. Acta* **2016**, *195*, 94–105.
- [42] W. Chen, X. Yu, Z. Zhao, S. Ji, L. Feng, *Electrochim. Acta* **2019**, *298*, 313–320.
- [43] X. Yu, C. Pei, W. Chen, L. Feng, *Electrochim. Acta* **2018**, *272*, 119–126.
- [44] P. Zhang, M. Chen, X. Shen, Q. Wu, X. Zhang, L. Huan, G. Diao, *Electrochim. Acta* **2016**, *204*, 92–99.
- [45] Q. Zhou, D. Wang, Y. Lian, S. Hou, C. Ban, Z. Wang, J. Zhao, H. Zhang, *Electrochim. Acta* **2020**, *354*, 136677.
- [46] M. Du, Q. Li, H. Pang, *J. Colloid Interface Sci.* **2020**, *580*, 614–622.
- [47] X. Guo, S. Wang, B. Yang, Y. Xu, Y. Liu, H. Pang, *J. Colloid Interface Sci.* **2020**, *561*, 801–807.
- [48] N. Li, Y. Li, Q. Li, Y. Zhao, C. S. Liu, H. Pang, *J. Colloid Interface Sci.* **2021**, *581*, 709–718.
- [49] Z. Li, X. Ji, J. Han, Y. Hu, R. Guo, *J. Colloid Interface Sci.* **2016**, *477*, 46–53.
- [50] D. Wang, Z. Xu, Y. Lian, C. Ban, H. Zhang, *J. Colloid Interface Sci.* **2019**, *542*, 400–409.
- [51] X. Deng, K. Zou, P. Cai, B. Wang, H. Hou, G. Zou, X. Ji, *Small Methods* **2020**, *4*, 2000401.
- [52] T. Zhang, F. Wang, L. Yang, H. Li, J. Chen, B. Yang, J. Lang, X. Yan, *New J. Chem.* **2020**, *44*, 1865–1871.
- [53] K. Zou, P. Cai, C. Liu, J. Li, X. Gao, L. Xu, G. Zou, H. Hou, Z. Liu, X. Ji, *J. Mater. Chem. A* **2019**, *7*, 13540–13549.
- [54] P. Wang, B. Yang, G. Zhang, L. Zhang, H. Jiao, J. Chen, X. Yan, *Chem. Eng. J.* **2018**, *353*, 453–459.
- [55] W. Sun, W. Zhao, S. Yuan, L. Zhang, Y. Yang, P. Ge, X. Ji, *Adv. Funct. Mater.* **2021**, DOI: <https://doi.org/10.1002/adfm.202100156>.
- [56] B. Yang, J. Chen, S. Lei, R. Guo, H. Li, S. Shi, X. Yan, *Adv. Energy Mater.* **2018**, *8*, 1702409.

- [57] N. Díez, G. A. Ferrero, A. B. Fuertes, M. Sevilla, *Batteries & Supercaps* **2019**, *2*, 701–711.
- [58] W. Liu, X. Zhang, Y. Xu, C. Li, K. Wang, X. Sun, F. Su, C. M. Chen, F. Liu, Z. S. Wu, Y. Ma, *Batteries & Supercaps* **2021**, *4*, 407–428.
- [59] S. Dong, L. Shen, H. Li, P. Nie, Y. Zhu, Q. Sheng, X. Zhang, *J. Mater. Chem. A* **2015**, *3*, 21277–21283.
- [60] J. Chen, B. Yang, H. Hou, H. Li, L. Liu, L. Zhang, X. Yan, *Adv. Energy Mater.* **2019**, *9*, 1803894.
- [61] Y. M. Chang, H. W. Lin, L. J. Li, H. Y. Chen, *Mater. Today* **2020**, *6*, 100054.
- [62] Y. Ding, B. Yang, J. Chen, L. Zhang, J. Li, Y. Li, X. Yan, *Sci. China Mater.* **2017**, *61*, 285–295.
- [63] K. Liao, H. Wang, L. Wang, D. Xu, M. Wu, R. Wang, B. He, Y. Gong, X. Hu, *Nanoscale Adv.* **2019**, *1*, 746–756.
- [64] Y. Ding, Y. Li, J. Li, X. Yan, *Chin. Chem. Lett.* **2020**, *31*, 2219–2224.
- [65] C. Yang, M. Zhang, N. Kong, J. Lan, Y. Yu, X. Yang, *ACS Sustainable Chem. Eng.* **2019**, *7*, 9291–9300.
- [66] J. Ding, H. Wang, Z. Li, K. Cui, D. Karpuzov, X. Tan, A. Kohandehghan, D. Mitlin, *Energy Environ. Sci.* **2015**, *8*, 941–955.
- [67] H. Liu, X. Liu, H. Wang, Y. Zheng, H. Zhang, J. Shi, W. Liu, M. Huang, J. Kan, X. Zhao, D. Li, *ACS Sustainable Chem. Eng.* **2019**, *7*, 12188–12199.
- [68] G. Dong, H. Wang, W. Liu, J. Shi, S. Sun, D. Li, H. Zhang, Y. Yang, Y. Cui, *ACS Appl. Mater. Interfaces* **2018**, *1*, 5636–5645.
- [69] D. Li, C. Ye, X. Chen, S. Wang, H. Wang, *J. Power Sources* **2018**, *382*, 116–121.
- [70] T. Huang, Z. Liu, F. Yu, F. Wang, D. Li, L. Fu, Y. Chen, H. Wang, Q. Xie, S. Yao, Y. Wu, *ACS Appl. Mater. Interfaces* **2020**, *12*, 52635–52642.
- [71] L. Chen, W. Duan, B. Yang, B. Liu, H. Li, J. Lang, J. Chen, *ChemistrySelect* **2020**, *5*, 5824–5830.
- [72] T. Palaniselvam, B. Babu, H. Moon, I. Hasa, A. L. Santhosha, M. Goktas, Y. N. Sun, L. Zhao, B. H. Han, S. Passerini, A. Balducci, P. Adelhelm, *Batteries & Supercaps* **2020**, *4*, 173–182.
- [73] J. Ding, Z. Li, K. Cui, S. Boyer, D. Karpuzov, D. Mitlin, *Nano Energy* **2016**, *23*, 129–137.
- [74] S. Liu, F. Hu, W. Shao, W. Zhang, T. Zhang, C. Song, M. Yao, H. Huang, X. Jian, *Nano-Micro Lett.* **2020**, *12*, 135.
- [75] N. Kurra, M. Alhabeb, K. Maleski, C.-H. Wang, H. N. Alshareef, Y. Gogotsi, *ACS Energy Lett.* **2018**, *3*, 2094–2100.
- [76] A. Brady, K. Liang, V. Q. Vuong, R. Sacci, K. Prenger, M. Thompson, R. Matsumoto, P. Cummings, S. Irle, H. W. Wang, M. Naguib, *ACS Nano* **2021**, *15*, 2994–3003.
- [77] Z. Fan, C. Wei, L. Yu, Z. Xia, J. Cai, Z. Tian, G. Zou, S. X. Dou, J. Sun, *ACS Nano* **2020**, *14*, 867–876.
- [78] M. Q. Zhao, X. Xie, C. E. Ren, T. Makaryan, B. Anasori, G. Wang, Y. Gogotsi, *Adv. Mater.* **2017**, *29*, 1702410.
- [79] D. Han, J. Zhang, Z. Weng, D. Kong, Y. Tao, F. Ding, D. Ruan, Q.-H. Yang, *Mater. Today* **2019**, *11*, 30–45.
- [80] H. J. Kang, Y. S. Huh, W. B. Im, Y. S. Jun, *ACS Nano* **2019**, *13*, 11935–11946.
- [81] P. Ma, D. Fang, Y. Liu, Y. Shang, Y. Shi, H. Y. Yang, *Adv. Sci.* **2021**, DOI: 10.1002/advs.202003185.
- [82] J. Luo, J. Zheng, J. Nai, C. Jin, H. Yuan, O. Sheng, Y. Liu, R. Fang, W. Zhang, H. Huang, Y. Gan, Y. Xia, C. Liang, J. Zhang, W. Li, X. Tao, *Adv. Funct. Mater.* **2019**, *29*, 1808107.
- [83] J. Luo, C. Fang, C. Jin, H. Yuan, O. Sheng, R. Fang, W. Zhang, H. Huang, Y. Gan, Y. Xia, C. Liang, J. Zhang, W. Li, X. Tao, *J. Mater. Chem. A* **2018**, *6*, 7794–7806.
- [84] W. Feng, R. R. Maca, V. Etacheri, *ACS Appl. Mater. Interfaces* **2020**, *12*, 4443–4453.
- [85] H. Li, J. Lang, S. Lei, J. Chen, K. Wang, L. Liu, T. Zhang, W. Liu, X. Yan, *Adv. Funct. Mater.* **2018**, *28*, 1800757.
- [86] Y.-E. Zhu, L. Yang, J. Sheng, Y. Chen, H. Gu, J. Wei, Z. Zhou, *Adv. Energy Mater.* **2017**, *7*, 1701222.
- [87] H. Zhai, B. Y. Xia, H. S. Park, *J. Mater. Chem. A* **2019**, *7*, 22163–22188.
- [88] Y. Li, H. Wang, L. Wang, R. Wang, B. He, Y. Gong, X. Hu, *Energy Storage Mater.* **2019**, *23*, 95–104.
- [89] L. Shen, Y. Wang, H. Lv, S. Chen, P. A. van Aken, X. Wu, J. Maier, Y. Yu, *Adv. Mater.* **2018**, *30*, 1804378.
- [90] J. Wang, J. Tang, B. Ding, V. Malgras, Z. Chang, X. Hao, Y. Wang, H. Dou, X. Zhang, Y. Yamauchi, *Nat. Commun.* **2017**, *8*, 15717.
- [91] R. Jia, G. Shen, D. Chen, *Sci. China Mater.* **2019**, *63*, 185–206.
- [92] S. Liu, Z. Luo, G. Tian, M. Zhu, Z. Cai, A. Pan, S. Liang, *J. Power Sources* **2017**, *363*, 284–290.
- [93] Z. Le, F. Liu, P. Nie, X. Li, X. Liu, Z. Bian, G. Chen, H. B. Wu, Y. Lu, *ACS Nano* **2017**, *11*, 2952–2960.
- [94] C. Liu, M. Zhang, X. Zhang, B. Wan, X. Li, H. Gou, Y. Wang, F. Yin, G. Wang, *Small* **2020**, *16*, 2004457.
- [95] L. Huang, L. Zeng, J. Zhu, L. Sun, L. Yao, L. Deng, P. Zhang, *J. Power Sources* **2021**, *493*, 229678.
- [96] R. Wang, S. Wang, Y. Zhang, D. Jin, X. Tao, L. Zhang, *J. Mater. Chem. A* **2018**, *6*, 1017–1027.
- [97] R. Thangavel, A. G. Kannan, R. Ponraj, M.-S. Park, H. Choi, D.-W. Kim, Y.-S. Lee, *Adv. Mater. Interfaces* **2018**, *5*, 1800472.
- [98] T. Wei, G. Yang, C. Wang, *ACS Appl. Mater. Interfaces* **2017**, *9*, 31861–31870.
- [99] B. Babu, M. M. Shajumon, *J. Power Sources* **2017**, *353*, 85–94.
- [100] D. Bauer, A. J. Roberts, S. G. Patnaik, D. J. L. Brett, P. R. Shearing, E. Kendrick, N. Matsumi, J. A. Darr, *J. Electrochem. Soc.* **2018**, *165*, A1662–A1670.
- [101] S. Dong, L. Shen, H. Li, G. Pang, H. Dou, X. Zhang, *Adv. Funct. Mater.* **2016**, *26*, 3703–3710.
- [102] Z. Tong, S. Liu, Y. Zhou, J. Zhao, Y. Wu, Y. Wang, Y. Li, *Energy Storage Mater.* **2018**, *13*, 223–232.
- [103] Y. Li, H. Wang, L. Wang, Z. Mao, R. Wang, B. He, Y. Gong, X. Hu, *Small* **2019**, *15*, 1804539.
- [104] H. Kim, E. Lim, C. Jo, G. Yoon, J. Hwang, S. Jeong, J. Lee, K. Kang, *Nano Energy* **2015**, *16*, 62–70.
- [105] H. Li, Y. Zhu, S. Dong, L. Shen, Z. Chen, X. Zhang, G. Yu, *Chem. Mater.* **2016**, *28*, 5753–5760.
- [106] E. Lim, C. Jo, M. S. Kim, M.-H. Kim, J. Chun, H. Kim, J. Park, K. C. Roh, K. Kang, S. Yoon, J. Lee, *Adv. Funct. Mater.* **2016**, *26*, 3711–3719.
- [107] L. Wang, X. Bi, S. Yang, *Adv. Mater.* **2016**, *28*, 7672–7679.
- [108] S. Qian, H. Yu, X. Cheng, R. Zheng, H. Zhu, T. Liu, M. Shui, Y. Xie, J. Shu, *J. Mater. Chem. A* **2018**, *6*, 17389–17400.
- [109] C. Zhao, C. Yu, M. Zhang, Q. Sun, S. Li, M. Norouzi Banis, X. Han, Q. Dong, J. Yang, G. Wang, X. Sun, J. Qiu, *Nano Energy* **2017**, *41*, 66–74.
- [110] Y. Li, H. Wang, B. Huang, L. Wang, R. Wang, B. He, Y. Gong, X. Hu, *J. Mater. Chem. A* **2018**, *6*, 14742–14751.
- [111] H. Wang, D. Xu, G. Jia, Z. Mao, Y. Gong, B. He, R. Wang, H. J. Fan, *Energy Storage Mater.* **2020**, *25*, 114–123.
- [112] X. Wu, C. Qian, H. Wu, L. Xu, L. Bu, Y. Piao, G. Diao, M. Chen, *Chem. Commun.* **2020**, *56*, 7629–7632.
- [113] R. Zhao, Y. Han, W. Li, J. Li, M. Chen, L. Chen, *Chem. Commun.* **2020**, *56*, 6798–6801.
- [114] Y. Lian, D. Wang, S. Hou, C. Ban, J. Zhao, H. Zhang, *Electrochim. Acta* **2020**, *330*, 135204.
- [115] Q.-T. Xu, H.-G. Xue, S.-P. Guo, *Electrochim. Acta* **2018**, *292*, 1–9.
- [116] M. Hu, Z. Ju, Z. Bai, K. Yu, Z. Fang, R. Lv, G. Yu, *Small Methods* **2020**, *4*, 1900673.
- [117] H. Wu, X. Zhang, Q. Wu, Y. Han, X. Wu, P. Ji, M. Zhou, G. Diao, M. Chen, *Chem. Commun.* **2019**, *56*, 141–144.
- [118] Y. Liu, J. Han, L. Fan, Y. Li, R. Guo, *Chem. Commun.* **2019**, *55*, 8064–8067.
- [119] J. Xie, Y. Pei, L. Liu, S. Guo, J. Xia, M. Li, Y. Ouyang, X. Zhang, X. Wang, *Electrochim. Acta* **2017**, *254*, 246–254.
- [120] N. Chen, C. Han, R. Shi, L. Xu, H. Li, Y. Liu, J. Li, B. Li, *Electrochim. Acta* **2018**, *283*, 36–44.
- [121] X. Zhao, H.-E. Wang, Y. Yang, Z. G. Neale, R. C. Massé, J. Cao, W. Cai, J. Sui, G. Cao, *Energy Storage Mater.* **2018**, *12*, 241–251.
- [122] R. Wang, S. Wang, X. Peng, Y. Zhang, D. Jin, P. K. Chu, L. Zhang, *ACS Appl. Mater. Interfaces* **2017**, *9*, 32745–32755.
- [123] J. Liu, Y. G. Xu, L. B. Kong, *J. Colloid Interface Sci.* **2020**, *575*, 42–53.
- [124] J. Liu, Y.-G. Xu, L.-B. Kong, *J. Ionics* **2021**, *27*, 1781–1794.
- [125] S. Li, W. He, B. Liu, J. Cui, X. Wang, D.-L. Peng, B. Liu, B. Qu, *Energy Storage Mater.* **2020**, *25*, 636–643.
- [126] S. Li, J. Chen, J. Xiong, X. Gong, J. Ciou, P. S. Lee, *Nano-Micro Lett.* **2020**, *12*, 34.
- [127] X. Hu, Y. Liu, J. Chen, J. Jia, H. Zhan, Z. Wen, *J. Mater. Chem. A* **2019**, *7*, 1138–1148.
- [128] J. Zhao, A. F. Burke, *Energy Storage Mater.* **2021**, *36*, 31–55.
- [129] M. Liu, J. Niu, Z. Zhang, M. Dou, Z. Li, F. Wang, *J. Power Sources* **2019**, *414*, 68–75.
- [130] K. Ramakrishnan, C. Nithya, R. Karvembu, *ACS Appl. Mater. Interfaces* **2018**, *1*, 841–850.
- [131] H. Chen, C. Dai, Y. Li, R. Zhan, M.-Q. Wang, B. Guo, Y. Zhang, H. Liu, M. Xu, S.-j. Bao, *J. Mater. Chem. A* **2018**, *6*, 24860–24868.
- [132] P. Cai, K. Zou, X. Deng, B. Wang, M. Zheng, L. Li, H. Hou, G. Zou, X. Ji, *Adv. Energy Mater.* **2021**, DOI: 10.1002/aenm.202003804.
- [133] H. Zhang, M. Hu, Z.-H. Huang, F. Kang, R. Lv, *Prog. Nat. Sci.* **2020**, *30*, 13–19.

- [134] F. Hu, S. Liu, S. Li, C. Liu, G. Yu, C. Song, W. Shao, T. Zhang, X. Jian, J. *Energy Chem.* **2021**, *55*, 304–312.
- [135] K. Zou, W. Deng, P. Cai, X. Deng, B. Wang, C. Liu, J. Li, H. Hou, G. Zou, X. Ji, *Adv. Funct. Mater.* **2021**, *31*, 2005581.
- [136] K. Zou, P. Cai, B. Wang, C. Liu, J. Li, T. Qiu, G. Zou, H. Hou, X. Ji, *Nano-Micro Lett.* **2020**, *12*, 121.
- [137] M. Biswal, A. Banerjee, M. Deo, S. Ogale, *Energy Environ. Sci.* **2013**, *6*, 1249–1259.
- [138] Y. Sun, J. Tang, F. Qin, J. Yuan, K. Zhang, J. Li, D.-M. Zhu, L.-C. Qin, J. *Mater. Chem. A* **2017**, *5*, 13601–13609.
- [139] X. Xie, M.-Q. Zhao, B. Anasori, K. Maleski, C. E. Ren, J. Li, B. W. Byles, E. Pomerantseva, G. Wang, Y. Gogotsi, *Nano Energy* **2016**, *26*, 513–523.
- [140] J. Zhao, G. Wang, R. Hu, K. Zhu, K. Cheng, K. Ye, D. Cao, Z. Fan, J. *Mater. Chem. A* **2019**, *7*, 4047–4054.
- [141] J. Xu, Z. Liu, F. Zhang, J. Tao, L. Shen, X. Zhang, *RSC Adv.* **2020**, *10*, 7780–7790.
- [142] R. Kiruthiga, C. Nithya, R. Karvembu, B. Venkata Rami Reddy, *Electrochim. Acta* **2017**, *256*, 221–231.
- [143] H. Zhang, M. Hu, Q. Lv, Z. H. Huang, F. Kang, R. Lv, *Small* **2020**, *16*, e1902843.
- [144] H. Wang, C. Zhu, D. Chao, Q. Yan, H. J. Fan, *Adv. Mater.* **2017**, *29*, 1702093.
- [145] H. Li, L. Peng, Y. Zhu, X. Zhang, G. Yu, *Nano Lett.* **2016**, *16*, 5938–5943.
- [146] Y. Dall'Agnese, P. L. Taberna, Y. Gogotsi, P. Simon, *J. Phys. Chem. Lett.* **2015**, *6*, 2305–2309.
- [147] H. J. Yoon, M. E. Lee, N. R. Kim, S. J. Yang, H.-J. Jin, Y. S. Yun, *Electrochim. Acta* **2017**, *242*, 38–46.
- [148] D. Xu, D. Chao, H. Wang, Y. Gong, R. Wang, B. He, X. Hu, H. J. Fan, *Adv. Energy Mater.* **2018**, *8*, 1702769.
- [149] B. Li, J. Zheng, H. Zhang, L. Jin, D. Yang, H. Lv, C. Shen, A. Shellikeri, Y. Zheng, R. Gong, J. P. Zheng, C. Zhang, *Adv. Mater.* **2018**, *30*, 1705670.
- [150] H. J. Kim, H. V. Ramasamy, G. H. Jeong, V. Aravindan, Y. S. Lee, *ACS Appl. Mater. Interfaces* **2020**, *12*, 10268–10279.
- [151] S. Wang, J. Zhao, L. Wang, X. Liu, Y. Wu, J. Xu, *Ionics* **2015**, *21*, 2633–2638.
- [152] J. Xu, M. Wang, N. P. Wickramaratne, M. Jaroniec, S. Dou, L. Dai, *Adv. Mater.* **2015**, *27*, 2042–2048.
- [153] R. Qiu, R. Fei, J.-Z. Guo, R. Wang, B. He, Y. Gong, X.-L. Wu, H. Wang, J. *Power Sources* **2020**, *466*, 228249.
- [154] H. Gu, L. Kong, H. Cui, X. Zhou, Z. Xie, Z. Zhou, *J. Energy Chem.* **2019**, *28*, 79–84.
- [155] D. Ma, L.-L. Zhang, T. Li, C. Liu, G. Liang, Y.-X. Zhou, X.-L. Yang, *Electrochim. Acta* **2018**, *283*, 1441–1449.
- [156] K. Kaliyappan, M. A. Jauhar, L. Yang, Z. Bai, A. Yu, Z. Chen, *Electrochim. Acta* **2019**, *327*, 134959.
- [157] Z. Xu, F. Xie, J. Wang, H. Au, M. Tebyetekerwa, Z. Guo, S. Yang, Y. S. Hu, M. M. Titirici, *Adv. Funct. Mater.* **2019**, *29*, 19003895.
- [158] S. Wang, R. Wang, Y. Zhang, D. Jin, L. Zhang, *J. Power Sources* **2018**, *379*, 33–40.
- [159] L. Zhang, J. Sun, H. Zhao, Y. Sun, L. Dai, F. Yao, Y. Fu, J. Zhu, *J. Power Sources* **2020**, *475*, 228679.
- [160] J. Kan, H. Wang, H. Zhang, J. Shi, W. Liu, D. Li, G. Dong, Y. Yang, R. Gao, *Electrochim. Acta* **2019**, *304*, 192–201.

Manuscript received: February 8, 2021

Revised manuscript received: April 3, 2021

Accepted manuscript online: April 11, 2021

Version of record online: April 29, 2021